A dissolved cobalt plume in the oxygen minimum zone of the Eastern Tropical South Pacific

N. J. Hawco,[1,2] D.C. Ohnemus,[3] J. A. Resing,[4] B. S. Twining[3] and M. A. Saito[2]

[1] MIT/WHOI Joint Program in Oceanography/Applied Ocean Science and Engineering, Woods Hole, MA, USA
[2] Department of Marine Chemistry and Geochemistry, Woods Hole Oceanographic Institution, Woods Hole, MA, USA
[3] Bigelow Laboratory for Ocean Sciences, East Boothbay, ME, USA
[4] Joint Institute for the Study of the Atmosphere and the Ocean, University of Washington and NOAA-PMEL, Seattle, WA, USA

Correspondence to: M. A. Saito (msaito@whoi.edu)

Abstract. Cobalt is a nutrient to phytoplankton, but knowledge about its biogeochemical cycling is limited, especially in the Pacific Ocean. Here, we report sections of dissolved cobalt and labile dissolved cobalt from the US GEOTRACES GP16 transect in the South Pacific. The cobalt distribution is closely tied to the extent and intensity of the oxygen minimum zone in the eastern South Pacific with highest concentrations measured at the oxycline near the Peru margin. Below 200 m, remineralization and circulation produce an inverse relationship between cobalt and dissolved oxygen that extends throughout the basin. Within the oxygen minimum zone, elevated concentrations of labile cobalt are generated by input from coastal sources and reduced scavenging at low O_2. As these high cobalt waters are upwelled and advected offshore, phytoplankton export returns cobalt to low-oxygen water masses underneath. West of the Peru upwelling region, dissolved cobalt is less than 10 pM in the euphotic zone and strongly bound by organic ligands. Because the cobalt nutricline within the South Pacific gyre is deeper than in oligotrophic regions in the North and South Atlantic, cobalt involved in sustaining phytoplankton productivity in the gyre is heavily recycled and ultimately arrives from lateral transport of upwelled waters from the eastern margin. In contrast to large coastal inputs, atmospheric deposition and hydrothermal vents along the Eastern Pacific Rise appear to be minor sources of cobalt. Overall, these results demonstrate that oxygen biogeochemistry exerts a strong influence on cobalt cycling.

Keywords. Cobalt, oxygen minimum zone, scavenging, GEOTRACES, hydrothermal vents, manganese oxides, phytoplankton, South Pacific, Peru Upwelling, micronutrient

1. Introduction

Cobalt is one of the least abundant inorganic nutrients in seawater and its scarcity may affect phytoplankton growth in certain regions (Moore et al., 2013). In the high macronutrient waters of the Costa Rica upwelling dome, for instance, Co and iron (Fe) amendments to surface seawater increased phytoplankton production more than Fe alone, promoting growth of the cyanobacterium *Synechococcus* (Ahlgren et al., 2014; Saito et al., 2005). While eukaryotic phytoplankton mainly use cobalt to compensate for insufficient zinc (Sunda and Huntsman, 1995), populating the same enzymes with either metal (Yee and Morel, 1996), marine cyanobacteria have an absolute growth requirement for Co that cannot be substituted, which suggests they may be more prone to limitation (Saito et al., 2002). Yet, the extent to which their

growth *in situ* is affected by cobalt scarcity ultimately depends on the processes that add Co to, or remove it from, the surface ocean relative to other limiting nutrients.

Biological cycling of dissolved cobalt (dCo) is apparent in vertical profiles, showing uptake and export in the surface and regeneration in the thermocline (Bown et al., 2011; Dulaquais et al., 2014a; Noble et al., 2012). While dCo in the euphotic zone can be entirely bound by strong organic ligands, a substantial portion (10–50 %) of subsurface dCo is unbound and labile (LCo, Bown et al., 2012; Ellwood and van den Berg, 2001; Saito and Moffett, 2001; Saito et al., 2005) and therefore vulnerable to scavenging (Moffett and Ho, 1996). The similar ionic radii and redox potentials of cobalt and manganese (Mn) cause dCo to be incorporated into authigenic Mn-oxides, which sink from the water column and accumulate in marine sediments (Cowen and Bruland, 1985; Moffett and Ho, 1996; Swanner et al., 2014). Below the euphotic zone, the persistence of labile dissolved cobalt throughout the Atlantic indicates that scavenging of dCo, unlike Fe, is slow (Noble et al., 2012). On timescales of ocean circulation, however, scavenging is responsible for decreasing dCo concentrations with depth and for the low ratio between dCo and macronutrients in deep waters relative to phytoplankton biomass (Moore et al., 2013). As these deep waters are repackaged into thermocline water masses and eventually brought to the surface (Sarmiento et al., 2011), the upper ocean would become depleted in cobalt – as well as other hybrid metals like Fe and Mn – without external sources that keep pace with scavenging (Bruland and Lohan, 2003; Noble et al., 2008).

Yet, the nature of marine cobalt sources is uncertain. In zonal sections of the North and South Atlantic, sources appear to be concentrated along continental margins (Noble and Saito, in prep;

Noble et al., 2012). In the western Atlantic, dCo concentrations exceeding 100 pM were associated with the flow of Upper Labrador Seawater, likely gained through intense sediment resuspension along the shelf or input prior to subduction (Noble and Saito, In prep). dCo in fresh and estuarine waters can be 100–1000x greater than seawater (Gaillardet et al., 2003; Knauer et al., 1982; Tovar-Sánchez et al., 2004) and Co is less prone to flocculation in estuaries than other metals (Sholkovitz and Copland, 1982). Terrigenous inputs from the American continent can be clearly seen in lower salinity surface waters influenced by the Gulf Stream (Noble and Saito, in prep; Saito and Moffett, 2002) and Amazon discharge (Dulaquais et al., 2014b). Yet, in both the North and South Atlantic, a much larger dCo plume was associated with the oxygen minimum zones along the Mauritanian and Namibian coasts (Noble and Saito, in prep, Noble et al., 2012). Although these waters are not anoxic, the dCo plumes imply that O_2 over the continental shelf is sufficiently low that reductive dissolution of Mn and Fe oxides in sediments releases a large flux of dCo to the water column (Heggie and Lewis, 1984; Sundby et al., 1986). Drawing from large inventories in the Atlantic OMZs, upwelling along eastern margins provides a large dCo flux to the surface ocean. While surface dCo maxima from atmospheric deposition generally do not appear in vertical profiles, this process may be important for regions that are isolated from continental input or receive very high levels of dust (e.g. the Sargasso Sea, Dulaquais et al., 2014a; Shelley et al., 2012).

To date, sectional datasets for dCo have been confined to the Atlantic and, as such, our understanding of cobalt cycling may be biased by the dominant processes occurring there. In comparison, the South Pacific receives considerably less dust deposition and river input (Mahowald et al., 2005; Milliman and Farnsworth, 2011), but hosts a much larger and more

reducing oxygen minimum zone. Surface transects off Peru and the Costa Rica Dome suggest a large source from upwelling (Ahlgren et al., 2014; Saito et al., 2004, 2005); however, profiles in the tropical Pacific are sparse (Noble et al., 2008; Saito et al., 2014). We measured the concentration of dissolved cobalt and labile dissolved cobalt in over 750 samples collected onboard the 2013 US GEOTRACES GP16 expedition across the South Pacific along 12° S, intersecting coastal upwelling along the Peru margin, hydrothermal venting over the East Pacific Rise, and oligotrophic conditions near Polynesia (Fig. 1). Across this section, the distribution of dCo and LCo follow the intensity of the oxygen minimum zone, with highest concentrations near the South American shelf and low concentrations in both deep waters and oligotrophic surface waters, matching OMZ-associated plumes observed in the Atlantic.

2. Methods

2.1 Sample collection and handling

Sampling on GP16 was conducted with a 24-position trace metal clean titanium rosette attached to a non-metallic Kevlar cable designed for the U.S. GEOTRACES program (Cutter and Bruland, 2012). An additional sample was collected from a surface towfish at each station. Subsamples were collected in a Class-100 sampling van from 12 L Go-Flo bottles (General Oceanics) and passed through 0.2 μM Acropack filters (Pall). All bottles were rinsed 3x with sample seawater before being filled entirely, leaving no headspace. For samples analyzed at sea, both dissolved and labile cobalt were analyzed from the same bottle. All samples were kept refrigerated at 4° C until analysis in a HEPA filtered clean van. All of the LCo samples and more than 90 % of dCo samples were analyzed at sea. Samples not analyzed at sea were preserved for dCo immediately after sampling using metal-free gas adsorbing satchels (Mitsubishi Gas

Chemical, model RP-3K), using 3–4 satchels per 6 seawater samples. Gas-impermeable plastic bags (Ampac) were heat sealed and were hand carried directly to Woods Hole at 4° C following disembarkation.

2.2 Cobalt determination by cathodic stripping voltammetry

dCo and LCo were measured using a cathodic stripping voltammetry (CSV) method optimized for organic speciation by Saito and Moffett, 2001. This method relies on the complexation of inorganic Co species by a strong synthetic ligand, dimethylglyoxime (DMG, $K^{cond} = 10^{11.5\pm0.3}$), which forms a bis-complex, $Co(DMG)_2$, with Co^{2+} that readily absorbs to a hanging mercury drop (Saito and Moffett, 2001). The $Co(DMG)_2$ complex is measured following a fast, 10 V s^{-1} sweep that reduces both the Co(II) to Co(0) and the DMG to 2,3-bis(hydroxylamino)butane, producing an 8–10 electron decrease in current for each $Co(DMG)_2$ complex (Baxter et al., 1998). The height of the $Co(DMG)_2$ reduction peak at -1.15 V is directly proportional to the Co concentration.

Triplicate scans of the seawater sample were followed by four standard cobalt additions (25 pM per addition) and the slope of their linear regression (mean $R^2 = 0.998$) was used to calculate the sample specific sensitivity (in nA pM^{-1}). The cobalt concentration was determined by dividing the mean of the three baseline peaks by the sensitivity, and correcting for reagent volume. The average deviation for these triplicate scans was 1.5 pM.

dCo analyses were conducted after a 1-hour UV oxidation procedure to remove strong organic ligands that prevent DMG from binding Co. UV digestion was performed in 15 mL quartz glass

tubes using a Metrohm 705 UV digester (Metrohm USA). Temperature was maintained below 20° C to minimize evaporation losses. After UV digestion, 11 mL of sample was pipetted into 15 mL polypropylene tubes and DMG and a buffering agent, EPPS, were added to final concentrations of 400 μM and 3.8 mM, respectively. 8.5 mL of sample solution was added to a Teflon analysis cup and mixed with 1.5 mL of 1.5 M $NaNO_2$, making a final analysis volume of 10 mL.

LCo was measured after >8 hour incubation of 11 mL of seawater with 400 μM DMG in a Teflon vial. LCo is therefore the concentration that will readily exchange with DMG. After this time, the sample was poured into an autosampler-compatible 15 mL poly-propylene tube (separate from those used for dCo analyses) and EPPS was added to 3.8 mM.

2.2.1 Preparing reagent and blanks

All bottles and sample tubes were soaked for >1 week in the acidic detergent Citranox, rinsed thoroughly with 18.2 MΩ water (Millipore), filled with 10 % trace metal grade HCl (J.T. Baker) to soak for 10 days, and rinsed thoroughly with ~10 mM TM-grade HCl. DMG (Sigma-Aldrich) was purified by recrystallization in a 1 mM EDTA solution (Sigma-Aldrich). Crystals were filtered, dried, and dissolved in HPLC grade methanol to a concentration of 0.1 M (Saito and Moffett, 2001). EPPS (Fischer) and Sodium Nitrite (Millipore) were both dissolved in 18.2 MΩ water to 0.5 M and 1.5 M, respectively, and treated with separate batches of thoroughly cleaned Chelex-100 beads (Bio-Rad) to remove background Co and Ni (Price et al., 1989). Standard additions of cobalt were generated by diluting a 1 ppm certified reference standard (SPEX

Certiprep) with 10 mM HCl to a concentration of 5.00 nM. 50 µl of this solution was added to the 10mL sample volume for each standard addition (25 pM addition).

To determine reagent blanks, Co-free seawater was generated by treating UV-seawater with cleaned Chelex-100 beads. The seawater was then UV digested a second time to remove any ligands leached during Chelex treatment. Any dCo measured in the Chelexed seawater derives from addition of Co from analytical reagents. The mean blank for at sea analysis was consistently low: 3.7 ± 1.2 pM (n = 28). For analyses at Woods Hole, mean blank was 4.7 ± 1.4 pM (n = 12). Blanks were subtracted from all measured values. Detection limits were calculated as triple the standard deviation of the blank: 3.6 pM for at-sea analyses and 4.2 pM for samples measured in Woods Hole.

2.2.2 Automated cobalt analyses

To accommodate a greater number of samples, our previous workflow (Noble et al., 2008) was modified to incorporate fully automated sample analyses using the Metrohm 858 Sample Processor autosampler. All measurements were performed using an Eco-Chemie µAutolabIII system connected to a Metrohm 663 VA stand. A hanging drop mercury electrode (Metrohm) was set to semi-hanging drop mode and accompanied by a 3 M KCl/AgCl reference electrode and glassy carbon auxiliary electrode. Scheduling and data acquisition were controlled using NOVA 1.8 software (Metrohm Autolab B.V). Automated delivery of seawater, sodium nitrite, and Co standard to the analysis cup was accomplished by three dedicated Dosino 800 burettes (Metrohm). Sample volume was increased to allow ~2 mL for conditioning tubing and analysis cup prior of sample delivery.

Tubes containing 11 mL seawater, DMG, and EPPS were inverted several times and placed onto a sampling rack where 8.5 mL of the mixture was dosed into the Teflon analysis cup. 1.5 mL of 1.5 M sodium nitrite was added directly to the sample cup. Samples were purged with high-purity N_2 (>99.99 %) for 180 s and then conditioned for 90 s at -0.6 V. Scan sweeps were run at 10 V s^{-1} from -0.6 V to -1.4 V. Before each analysis, the sample cup was rinsed fully with Milli-Q water and 1 mL sample before measurement. Between uses, autosampler tubes, quartz vials, and Teflon cups were rinsed with 10 mM HCl, 18.2 MΩ water, and 1-2 mL of new sample. The autosampler uptake line was rinsed with 10 mM HCl and 18.2 MΩ water when transitioning from LCo analyses to dCo analyses.

We noticed a decrease in sensitivity of preserved samples relative to those analyzed at sea, possibly caused by an increase in the sample pH during storage. Sensitivity was restored by doubling the concentration of our buffering agent, EPPS, in the sample to a final concentration of 7.6 mM. We tested a broad range of EPPS additions in UV seawater and found the cobalt concentration unchanged while the variance between triplicate scans was reduced markedly by the increase in sensitivity (data not shown). We tentatively attribute this decrease in sensitivity in preserved samples to CO_2 adsorption by gas satchels, which would increase sample pH.

2.2.3 Signal processing

Analyses conducted at sea were characterized with a mild to moderate electrical interference that mandated additional processing before peak height could be reliably measured (Fig. 2). We opted for a simplified least squared fitting routine included in the NOVA software package that

conducts a 15-point weighted moving average – equivalent to a 36.9 mV window – according to a 2nd order polynomial. This method did not distort measured peak height when noise was low (Fig. 2a, b). A small fraction of scans (~3 %) were not adequately fit using this routine and were instead smoothed using a 9-point linear moving average (22.1 mV window, Fig. 2c), also included in NOVA. For all samples, peak height was measured manually to minimize peak distortion due to added noise.

Subsequent analyses in the laboratory at Woods Hole were able to remove this signal by increasing the current sampling step from 2.46 mV (341 points between -0.6V to -1.4V) to 4.88 mV (174 points) which eliminated the need for smoothing prior to sample analysis. We observed good agreement between samples analyzed at sea and in the lab, indicating that the smoothing procedures applied at sea did not bias the data and that gas adsorbing satchels preserved original concentrations (Noble and Saito, in prep).

2.2.4 Intercalibration and internal laboratory standard

All data reported in this manuscript have been submitted to the Biological and Chemical Oceanography Data Management Center (BCO-DMO, http://www.bco-dmo.org/dataset/647250). Our laboratory continues to participate in international intercalibration efforts through the GEOTRACES program in anticipation of the release of the 2nd Intermediate Data Product, Summer 2017. The sampling scheme for GP16 included 2 overlapping samples per full depth profile where the shallowest sample of the deep cast matched the deepest sample for the mid cast, and the shallowest sample from the mid cast matched the deepest sample from the shallow cast (i.e. a 36-point profile is composed of 34 discreet depths and 2 overlapping

depths). Comparing overlapping samples collected at the same depth and location on separate hydrocasts provides a measure of reproducibility. The average difference between dCo analyses across 40 overlapping depth samples was 5.7 pM with a median difference of 3.5 pM. For labile cobalt, average deviation was 2.1 pM (median of 2.0 pM, n = 41). Least-squares regression of these samples yielded slopes close to 1(0.98 for dCo and 0.96 for LCo; y-intercept forced to 0), indicating good reproducability. Furthermore, comparisons with other groups measuring dCo in the same samples reported here suggest strong agreement between groups despite major methodological differences (C. Parker and K. Bruland, personal communication).

Because acidified community reference materials such as the SAFe standards require a delicate neutralization to pH 7.5–8 prior to analysis, a large batch of UV oligotrophic seawater was generated prior to the cruise and used to assess instrument performance during at-sea analysis. This consistency seawater standard was run ~3x per week, as were blanks, and values were stable over several reagent batches for the duration of the cruise (4.5 ± 2.1 pM, n = 28). SAFe standard D1 was measured at sea (48.5 ± 2.4 pM, n = 3) and fell within 1 SD of the consensus value (46.6 ± 4.8 pM). SAFe standard D2 and GEOTRACES standard GSP were run at higher frequency for analyses at Woods Hole. Our measurements of D2 (46.9 ± 3.0 pM, n = 7) agreed with consensus values (45.7 ± 2.9 pM) and concentrations from our lab published previously (Noble et al., 2012). While the GSP standard does not have a consensus value, our determinations (2.5 ± 2.0 pM, n = 10) are within the range for SAFe S (4.9 ± 1.2 pM), which was collected at the same offshore location as GSP. Acidified SAFe and GEOTRACES standards were neutralized with concentrated ammonium hydroxide (Seastar), mixing the entire sample between drops, prior to UV digestion. When base was added more quickly, measured dCo was

halved, presumably due to adsorption or co-precipitation onto magnesium hydroxides formed during base addition. For analysis of neutralized standards, we found a ~6:1 EPPS:NH_4OH (M:M) buffer improved pH stability during analysis and removed significant baseline drift observed with samples solely buffered with EPPS.

2.3 Particulate metal analyses

Particulate material collected from Go-Flo bottles was filtered onto acid-cleaned 0.45 μm polyethersulfone filters (25 mm). Digestion protocol and analyses are identical to those used to measure particulate metal concentrations during the North Atlantic GA03 cruise, described in Twining et al., 2015. After filtration, filters were halved, digested at 135° C in sealed Teflon vials containing 4 M HCL, 4 M HNO_3, and 4 M HF; digests were then dried, and re-dissolved in 0.32 M HNO_3 before analysis. pCo, pMn and pP concentrations were measured by ICP-MS (Element 2, Thermo Scientific), calibrated using external multi-element standard curves, and corrected for instrument drift and sample recovery by In and Cs internal standards. More detailed methods for this dataset can be found elsewhere (Ohnemus et al., In Press).

3. Results

We report 680 determinations of dissolved cobalt (dCo) and 783 determinations of labile dissolved cobalt (LCo) measured at sea, onboard the GP16 expedition in October–December 2013, as well as an additional 140 measurements of dCo measured from preserved samples on land. In this section, we describe the distributions of dCo, particulate cobalt (pCo), and LCo in the South Pacific Ocean.

3.1 Dissolved Cobalt

Throughout the GP16 transect, nutrient uptake and scavenging result in a hybrid-type profile for dissolved cobalt (dCo, Fig. 3), similar to dCo profiles from the Atlantic (Bown et al., 2011; Dulaquais et al., 2014b; Noble et al., 2012; Noble and Saito, in prep) and North Pacific (Ahlgren et al., 2014; Knauer et al., 1982; Saito et al., 2014). dCo ranged from <3 pM (below detection) in the South Pacific Gyre (e.g. Stations 23, 36) to 210 pM beneath the oxycline near the Peru Margin (Station 1). In the deep Pacific, concentrations fell between 20–40 pM but increased slightly at deepest stations below 4500 m. These values are much less than those observed in zonal transects surveying the North and South Atlantic (Noble et al., 2012; Noble and Saito, in prep) but are similar to measurements in the Southern Ocean (Bown et al., 2011), indicating that dCo is scavenged in the deep ocean along meridional overturning circulation. Below 3000 m, dCo is somewhat lower east of the Eastern Pacific Rise (EPR), and matches less oxygenated, older waters than in the western portion of the transect (Fig. 4). While many profiles west of the EPR show considerable variation between 2000–3000 m suggestive of hydrothermal influence, the range is small (<10 pM) relative to background concentrations (30–40 pM) and unlike the 50-fold excess of hydrothermal dFe and dMn above background seawater measured at Station 18 (Resing et al., 2015).

dCo peaks in the mesopelagic, typically between 300–500 m. Towards the Peru shelf, this maximum shoals and increases, following the position and intensity of the oxygen minimum zone (OMZ, defined here as <20 μM O_2). Although the OMZ is several hundred meters thick near the eastern margin (Fig. 3), dCo concentrations >100 pM are restricted to samples collected just below the oxycline. Despite this narrow depth range, >100 pM dCo extends as far as 100°

W. For all depths below 200 m, dCo follows a negative linear relationship with O_2 (Fig. 5a). Over the Peru shelf, maximum dCo was measured at the top of the OMZ and dCo decreased with depth (except for the shallowest and most shoreward Station 2). Only at the western edge of the section do dCo and O_2 decouple: the dCo maximum at Station 36 is deeper (500–1000 m) than the oxygen minimum (300–500 m), seemingly independent of the influence of the South Pacific OMZ (Fig. 3).

All profiles show a surface or near-surface minimum that indicates biological uptake and export. As a result, dCo is well traced by dissolved phosphate, PO_4, in the upper 200 m of the ETSP (Fig. 5c). This relationship holds despite sharp transitions to high dCo in the oxycline near the Peru shelf. Upwelling of O_2-depleted, PO_4-rich waters contributes to high dCo in the surface ocean along the eastern margin with concentrations decreasing westward due to mixing and export. A secondary surface dCo maximum marked a cyclonic eddy sampled at 89° W (Station 9, V. Sanial, personal communication), which appeared to transport a shelf-like dCo and LCo signature for the upper 300 m into the offshore OMZ (Figs. 6a, b). In the South Pacific gyre, dCo in the euphotic zone falls below 10 pM. While the lowest PO_4 was found in low salinity surface waters west of 140° W, minimum dCo and deepest nutriclines corresponded to a southwestward excursion in the transect between Stations 17–23 (109–120° W), which were accompanied by high salinities (>36) associated with the eastern part of the subtropical gyre. In contrast to the deep, smooth dCo nutricline further to the east, stations at the western edge of the section (Stations 32, 34, and 36) contained 20 pM Co until ~50 m where concentrations decrease sharply surfaceward, resembling profiles in the North Atlantic (Fig. 3; Noble and Saito, in prep).

3.2 Particulate Cobalt

The surface minimum in dCo is mirrored by a near-surface maximum in particulate cobalt (pCo) from biological uptake throughout the GP16 section. The distribution of pCo (Fig. 6c) resembles particulate phosphorus (pP), chlorophyll, and other indicators of phytoplankton biomass. Very high pCo (>10 pM) was measured in the highly productive waters in the Peru upwelling ecosystem while lower concentrations (2–4 pM) were found in oligotrophic surface waters. West of 100° W on the GP16 transect, a secondary pCo maximum between 300–500 m overlaps with high particulate Mn (pMn), reflecting Co incorporation into Mn-oxides in oxygenated thermocline waters (Fig. 6c). Elevated pCo was also found at the top of the OMZ in the eastern half of the transect, corresponding with high dCo from remineralization. High pP and low pMn in these samples suggest that pCo may be present as biomass in anoxic bacterial and archaeal communities (Ohnemus et al., In Press), rather than incorporation into bacterial Mn-oxides by co-oxidation. pMn increases sharply west of 100° W, implying that pCo here is present as an authigenic phase (Ohnemus et al., In Press; Moffett and Ho, 1996).

3.3 Labile Dissolved Cobalt

dCo can be bound by extremely strong organic ligands that affect its reactivity (Ellwood and van den Berg, 2001; Saito and Moffett, 2001). These ligands may be composed of degradation products of the cobalt-bearing cofactor vitamin B_{12} and may be stabilized following oxidation of Co(II) to Co(III) (Baars and Croot, 2015). Unlike other metals such as Fe, dCo bound to natural ligands is kinetically inert to ligand exchange (although some forms may still be bioavailable) and strong Co(II) ligands are not in excess of dCo, largely due to binding competition with nanomolar levels of labile nickel (Saito and Moffett, 2001; Saito et al., 2005). These properties

can result in a significant fraction of labile dissolved cobalt (LCo) that can be measured without the UV-oxidation procedure necessary to measure dCo, especially in the mesopelagic (Noble et al., 2012).

On GP16, the distribution of LCo is similar to that of dCo (Figs. 3, 4, 6). Except for samples from the upper 50 m, dCo and LCo form a linear relationship ($R^2 = 0.88$) whose slope indicates that ~33 % of dCo is labile (Fig. 7a). Major exceptions are confined to the highly productive waters over the Peru shelf (Stations 1–6) where LCo is much lower than expected from dCo. In these waters, LCo decreases in step with silicate (Fig. 7c). As in the North and South Atlantic (Noble et al., 2012; Noble and Saito, in prep), LCo is undetectable in the surface ocean outside of the waters influenced by upwelling (beyond 100° W, Fig. 6b). The absence of LCo from the upper 300 m of the water column is deeper than corresponding gradients in the Atlantic, suggesting cobalt depletion is more intense in the South Pacific.

In the deep Pacific (>3000 m), where dCo is low, LCo is undetectable. LCo remains low (<15 pM) in the mesopelagic, except where the OMZ is most intense (Fig. 4). Within the OMZ, LCo maxima coincide with dCo maxima (Stations 1–15), but further to the west these LCo maxima are much less pronounced and occur deeper than dCo maxima (Fig. 3). The LCo plume from the OMZ also extends deeper (below 2000 m) than the corresponding dCo (<2000 m), suggesting that remineralization and scavenging affect these quantities in different ways. Slight secondary maxima between 1500–2000 m (10–15 pM) appear in the center of the section on $\sigma_\theta = 27.7–8$ kg m^{-3} isopycnal layers (Fig. 4c, 105° W–115° W), perhaps tracing transport of LCo remineralized in the eastern basin as these waters flow over the mid ocean ridge.

4. Discussion

The most striking aspect of the dCo distribution in the ETSP is the very high concentrations present in the OMZ (Figs. 3–5). Similar distributions have been observed in both the North and South Atlantic, where >100 pM dCo plumes corresponded to low oxygen waters underneath the Benguela and Mauritanian upwelling systems (Noble et al., 2012; Noble and Saito, in prep). In the North Pacific, profiles from the Costa Rica Dome (Ahlgren et al., 2014), the California margin (Biller and Bruland, 2013; Knauer et al., 1982), and the Central Pacific along 155° W (Saito et al., 2014) support an OMZ-cobalt plume there as well. Based on measurements from these four OMZs, oxygen biogeochemistry seems to exert a major control on cobalt cycling throughout the oceans. It is interesting to note that the magnitude of the observed dCo plumes does not appear to scale with minimum O_2 between Atlantic and Pacific OMZs. While minimum O_2 in the Atlantic OMZs exceeds 20 μM, much of the ETSP is anoxic (Karstensen et al., 2008; Ulloa et al., 2012). Yet, dCo in the ETSP occupies a similar 100–200 pM range reported for the North and South Atlantic OMZs (Noble et al., 2012; Noble and Saito, in prep). Clearly, other factors besides O_2 alone contribute to large scale plumes of dissolved cobalt in the oceans.

In the following, we describe the oceanographic processes that lead to elevated dCo and LCo concentrations in low-oxygen waters (Section 4.1). At the basin scale, the combined effects of remineralization and circulation link dCo with O_2 throughout the water column in the ETSP (Section 4.1.1). The cobalt plume in the OMZ, however, is more than an extrapolation of these mechanisms, requiring a large coastal source (Section 4.1.2), and suppression of dCo scavenging at very low O_2 (Section 4.1.3). The mechanism, magnitude, and redox sensitivity of the coastal

Co source are then examined in greater detail (Section 4.2). Finally, we highlight the scarcity of dCo – a critical micronutrient to phytoplankton – in the surface ocean of the South Pacific and the dependence of surface ocean dCo supply on coastal sources (Section 4.3).

4.1. Processes generating the OMZ cobalt plume in the Eastern South Pacific Ocean

4.1.1 Basin-scale remineralization and circulation couple dCo with O_2

In the ETSP, tight coupling between dCo and O_2 is evident in the strong, inverse relationship that describes all samples below 200 m (Fig. 5a). In light of the nutrient-like dCo depletion in the surface of the ETSP and elsewhere (Fig. 6, Ahlgren et al., 2014; Dulaquais et al., 2014b; Noble et al., 2012), this negative correlation might be attributed to remineralization: dCo is returned to the dissolved phase from a sinking biogenic phase following respiration (i.e. O_2 consumption). The slope of the dCo:O_2 line (-0.33 μM M^{-1}, R^2 = 0.75 for 200–5500 m) would then represent the biological stoichiometry of the exported organic material in the ETSP. However, Co:P ratios in particulate material collected in the upper 50 m on GP16 indicate greater phytoplankton cobalt utilization (median pCo:pP of 140 μM M^{-1} ÷ 118 O_2:P M M^{-1} = 1.2 Co:O_2 μM M^{-1}; DeVries and Deutsch, 2014). If the dCo:O_2 trend is borne solely from remineralization, a greater slope would be expected, implying removal of dCo by scavenging. The linearity in the dCo:O_2 relationship is also not reproduced upon conversion of O_2 to apparent oxygen utilization (AOU = $O_{2,saturation}$ – $O_{2,\ measured}$, Fig. 5b, R^2 = 0.49), further suggesting that other factors besides remineralization (such as circulation and scavenging) shape the subsurface dCo distribution as well.

In the deep ocean, near-conservative mixing of low O_2/high dCo water masses with high O_2/low dCo water masses probably contributes to the observed dCo:O_2 relationship. The enormous

depth range (>5000 m) described by the linear dCo:O_2 relationship contrasts with the near-exponential decrease in remineralization rates with depth (e.g. Karstensen et al., 2008). It is likely that deep Pacific circulation acts to spread signals of local dCo remineralization throughout the water column, aggregating a multitude of export stoichiometries and remineralization processes into a single, coherent relationship across the basin. LCo is undetectable below ~2500 m and the shallower slope of the LCo:O_2 trend (-0.11 μM M^{-1}, R^2 = 0.67, not shown) implies that the dCo:O_2 relationship is driven mostly by strongly complexed species, which are less vulnerable to co-oxidation by Mn-oxidizing bacteria in the water column (Moffett and Ho, 1996). Since the deep Pacific can be broadly regarded as a mixture of oxygenated circumpolar waters and OMZs (especially from the North Pacific), the linear dCo:O_2 relationship between 200 and 5500 m may reflect mixing of a dCo pool that is largely inert to losses by scavenging.

In the upper 200 m, dCo is not well coupled with O_2 and almost all samples fall above the line established by deeper samples (Fig. 5a). Near the South American margin, the dCo maximum in the upper OMZ is more than twice the dCo concentration expected by extrapolation of the basin-scale dCo:O_2 relationship to the 0 μM O_2 intercept (77 pM, Fig. 5a). The similarity of dCo profiles to profiles of excess N_2 from denitrification from this region (e.g. Chang et al., 2010) implies that both the dCo maximum in the OMZ and its decrease with depth are driven by factors that also affect nitrogen loss: namely in-situ remineralization of sinking biogenic particles and lateral transport of coastal waters that experience high rates of denitrification and are also rich in dCo (DeVries et al., 2012).

4.1.2 Distinct surface and mesopelagic Co:P relationships

In the upper ocean (0–200 m), dCo is linearly related to PO_4 (Figs. 5c), indicating that the processes controlling PO_4 in the surface – upwelling, mixing, biological uptake and export – are the main drivers of dCo as well. In the upper 50 m, the dCo:PO_4 slope (69 μM:M, R^2 = 0.89, Fig. 7b) may describe export stoichiometry throughout the Eastern Pacific. That the surface dCo:PO_4 slope intercepts the highest dCo concentrations (below the 50 m depth range of the regression, Fig. 5c, cyan line) indicates that new cobalt sourced from the shelf is rapidly incorporated into the biological cycle and that the capacity for phytoplankton Co uptake is not overwhelmed by the order of magnitude higher dCo in coastal waters relative to the open ocean. Culture experiments with model diatoms and coccolithophores demonstrate this capacity (Shaked et al., 2006; Sunda and Huntsman, 1995; Yee and Morel, 1996), deploying Co to zinc enzymes to maintain activity when Zn becomes scarce. When Zn is limiting, Co quotas, as observed in open ocean phytoplankton, are 10–100x greater than Co quotas when Zn is replete (Sunda and Huntsman, 1992; Twining and Baines, 2013). Therefore, minor substitution of Zn quotas by Co (~10 %) can double cellular Co levels in eukaryotes, resulting in nearly complete uptake of dCo from the surface ocean.

A separate nutrient-like dCo:PO_4 trend arises from gradients of both elements in the open ocean nutricline (Fig. 5c). The slope of the mesopelagic trend (16 μM:M, for 200–1000 m, red line in Fig. 5c) is much less than that measured for the upper 50 m (69 μM:M, cyan line). Due to considerable preformed PO_4 in deep waters, as well as elevated dCo:PO_4 ratios in the OMZ, the mesopelagic dCo:PO_4 regression is less robust than in the surface (R^2 = 0.21), though the slope does reflect dCo and PO_4 covariation in this depth range when PO_4 is <2 μM (Fig. 5c, red line).

Regardless, there seems to be a fundamental mismatch between dCo:PO_4 from the upper water column (0–200 m) and that observed deeper (200–1000 m).

In the eastern margin, the surface and mesopelagic dCo:PO_4 vectors are joined at 2.6 μM PO_4 by a near-vertical line that makes the dCo:PO_4 domain triangular. Interpretation of this line depends largely on its perceived direction: a downward vector can be a fingerprint of scavenging while an upward vector describes a cobalt source (Noble et al., 2008; Saito et al., 2010). This ambiguity is clarified by examining dCo:PO_4 gradients within isopycnal surfaces, which strongly indicate a source at low O_2. In the ETSP, σ_θ 26.2 and 26.4 isopycnals host the upper OMZ and the oxygenated thermocline waters west of 100° W. Water masses on these surfaces can be distinguished on the basis of salinity; from the GP16 dataset, mixing between salty and deoxygenated equatorial sub-surface waters (ESSW or 13° C water) with fresher, ventilated Sub-Antarctic waters is apparent (Fiedler and Talley, 2006; Toggweiler et al., 1991). Oxygenated waters on σ_θ = 26.2 and 26.4 show a tight coupling between dCo and PO_4 from remineralization of both elements (Fig. 8a). For samples with <20 μM O_2, however, deviation from the oxic dCo:PO_4 trend is always positive, indicating a dCo source within the OMZ. When oxygen is low, dCo follows salinity (Fig. 8b). Mixing of high salinity (34.9–35.0), high dCo ESSW from the northeast with low salinity, low dCo Subantarctic waters explains the dCo:salinity covariation on these isopycnal surfaces. While ESSW is fed by the equatorial undercurrent (EUC), which originates near Papua New Guinea and transports a large Fe and Al source eastward (Slemons et al., 2010), it is low in dCo (as measured at 155° W, Hawco and Saito, unpublished; Saito et al., 2014). When the EUC bifurcates near the Galapagos, it mixes with

503 coastal waters north and south of the equator (Fiedler and Talley, 2006; Stramma et al., 2010),
504 where its high dCo signature is likely acquired.
505
506 **4.1.3 Suppression of cobalt scavenging in the OMZ**
507 The isopycnal dCo:salinity relationship implies cobalt scavenging in the OMZ is low (Fig. 8b).
508 This is not surprising given the slower rates of MnO_2 formation at low O_2 (Johnson et al., 1996;
509 von Langen et al., 1997) and very low particulate Mn measured in the ETSP OMZ (Ohnemus et
510 al. In Press). In the OMZ, both pCo:pP and pMn:pP ratios in the OMZ are consistent with
511 micronutrient use by microbial communities and resemble biomass collected in the euphotic
512 zone on GP16 (Co:P = 0.5–4 x 10^{-4} M M^{-1}, Mn:P ~10^{-3} M M^{-1}; Fig. 9, pink and cyan lines).
513 These low, biomass-like pCo:pP and pMn:pP signatures in the ETSP OMZ are consistent with
514 thermodynamic and kinetic barriers to Mn oxidation at very low O_2 (Ohnemus et al., In Review).
515
516 Crossing the anoxic/oxic transition at 100° W in the thermocline (σ_θ 26.2–27.0, centered at 300
517 m) results in a factor of ten higher pMn concentrations and implies a redox threshold to Mn
518 oxidation in the mesopelagic (Fig. 9, blue circles). Heterotrophic Mn-oxidizing bacteria are
519 known to incorporate Co by enzymatic co-oxidation into the Mn-oxide lattice and are prevalent
520 throughout the water column (Cowen and Bruland, 1985; Moffett and Ho, 1996). While
521 particulate Co profiles in the ETSP have a near-surface maximum from biological uptake (Fig.
522 6c), pCo attenuates much less with depth than pP in oxic thermocline waters. Very high pCo:pP
523 ratios (up to 10^{-3} M M^{-1}) are found in the oxygenated thermocline but not in the OMZ (Fig. 9,
524 pink circles). The coincidence of high pCo:pP and high pMn throughout the mesopelagic is
525 consistent with pCo being present in an authigenic Mn-oxide phase, marking an important

transition between nutrient-like cobalt cycling in the surface ocean (where pCo is almost entirely biogenic) to Mn-oxide driven scavenging at depth.

The stimulation of cobalt scavenging across the anoxic/oxic transition at 100° W was also reflected in a sharp decrease in LCo:PO_4 as scavenging removed LCo from the water column (Fig. 9, black circles). Indeed, the same oxygenated thermocline samples with high pMn and pCo:pP are responsible for the gradual slope in dCo:PO_4 space (16 μM M^{-1}, Fig. 5c, red line). The offset between high surface and low mesopelagic dCo:PO_4 is mirrored by the lower surface and higher mesopelagic pCo:pP. While scavenging is often presumed to draw chiefly from metals in the dissolved phase, the heterotrophic nature of Mn-oxidizing bacteria and their abundance in sediment traps hint that Mn-oxidizing bacteria may access biogenic metal pools within sinking particles (Cowen and Bruland, 1985). In such a case, pCo may be shunted directly from a biogenic to an authigenic phase without being truly remineralized, preventing the equal return of dCo at depth relative to that exported from the surface, as documented here by the disparity between deep and shallow dCo:PO_4 slopes (Fig. 5c). An important consequence of mesopelagic scavenging is that ventilation of these waters by upwelling without an exogenous source (e.g. the continental margin) would create conditions whereby dCo, relative to PO_4, is not supplied to the same extent it is presently utilized and exported. Because these scavenged waters are relatively shallow and have short ventilation ages (Fiedler and Talley, 2006), fluxes of cobalt to the South Pacific from margin sources must be large enough to balance these scavenging losses.

4.2 A major cobalt source from the Peruvian margin

549 **4.2.1 Water column signatures of a dCo source**

550 The strong covariation between high dCo and low O_2 in the ETSP and the intersection of the
551 OMZ with the South American margin suggests that the continental shelf may be an important
552 cobalt source. Sections from the North and South Atlantic (Noble et al., 2012; Noble and Saito,
553 in prep) and profiles from the North Pacific (Ahlgren et al., 2014; Knauer et al., 1982) have
554 resulted in similar assertions, but the coincidence of high phytoplankton productivity along
555 eastern margins also imprints signals from elevated remineralization. This is certainly the case
556 for the ETSP, where Stations 2 and 3 on the Peru shelf featured >1.5 μg chlorophyll L^{-1} in the
557 euphotic layer, and >4 μM nitrite throughout the OMZ from intensified anoxic remineralization.
558 As a result, the dCo profile in Peru shelf waters strongly resembles PO_4 and other nutrients
559 above the oxycline (Fig. 10). Unlike PO_4, however, these shelf stations show a dCo maximum at
560 the oxycline and decreasing concentrations with depth that more strongly resembles the Mn
561 profile (Fig. 10), implying that additional process contribute to the dCo profile over the shelf.
562
563 Positive correlations between dCo, LCo and dMn within the OMZ on the Peru shelf reflect a
564 shared source (Fig. 11). The slope of the LCo:dMn relationship (18 ± 2 mM M^{-1} R^2 = 0.76) is
565 nearly identical to that in upper continental crust and Andesite (21–26 mM M^{-1}, McLennan,
566 2001; Taylor and McLennan, 1995), matching expectations that mineral dissolution should
567 provide labile Co. However, the steeper slope for the dCo:dMn relationship (42 ± 5 mM M^{-1} R^2
568 = 0.67) exceeds crustal endmembers. Addition of a second, Co-enriched component is needed to
569 explain the observed relationship. Given the massive productivity over the Peru shelf, biological
570 export and remineralization of dCo and dMn in the OMZ is a reasonable cause for the high
571 Co:Mn ratio in the shelf OMZ. From particulate material in the upper 40 m of shelf stations (1–

5), the average Co:Mn ratio in local biomass is between 100 and 110 mM M^{-1} (median and mean), roughly 5 times higher than continental crust, and falling within the range reported for single cell analysis of phytoplankton cells from other regions (70–400 mM M^{-1}, Twining and Baines, 2013). The combination, then, of a high biotic Co:Mn and a lower ratio from a sedimentary source can produce the slope observed in the water column, but requires remineralized dCo to be chiefly ligand-bound in order to preserve the near-crustal LCo:Mn slope. The higher Co:Mn ratio in biomass relative to their shared sedimentary source also results in a nutrient trap that returns upwelled dCo to the OMZ more efficiently than dMn and implies that input of dCo from the shelf is rapidly followed by biological utilization, evident in the immediate transition from a dMn-like profile below the oxycline to a PO_4-like profile above it (Fig. 10).

Water column observations of a large dCo source are also mirrored in the depleted Co contents of continental shelf sediments along the Peru margin. A survey of continental shelf sediments underlying the Peru OMZ found low Co/Al ratios ($1.2 \pm 0.3 \times 10^{-4}$ g g^{-1}, Böning et al., 2004) relative to Andesitic and upper continental crusts (2.63 and 2.11×10^{-4} g g^{-1} respectively, McLennan, 2001; Taylor and McLennan, 1995), requiring that about half of the Co delivered to the continental shelf from crustal sources dissolved prior to long-term burial on the shelf. The only other element to have a similar depletion was Mn, which covaried with Co across all samples in the Böning et al. study, consistent with release of both metals by reductive dissolution. Yet the exact mechanism for dCo release is unclear: mass balance calculations for Mn indicate that diffusive fluxes from sediment porewaters on the Peru Shelf are much too slow to account for solid-phase Mn/Al deficits that accumulate in the sediment column (Scholz et al.

595 2011). Therefore, most Mn is released prior to sedimentation on the margin, either by dissolving
596 directly in the water column or through upstream release in estuaries. Since Co covaries with Mn
597 in both dissolved and sediment phases (Fig. 11, Böning et al., 2004), the ultimate source of the
598 dCo plume in the Peruvian OMZ may not be generated by diffusion from margin sediments
599 either.
600
601
602 **4.2.2 Potential redox sensitivity of coastal cobalt sources**
603 The Co/Al ratio in buried sediments on the continental shelf can provide a coarse measure of
604 how much Co has been released to the ocean. Sub-crustal Co/Al ratios in Peruvian sediments
605 between 9–14° S (Böning et al., 2004) match similar measurements in Chilean OMZ sediments
606 at 36° S (Table 2, Co/Al = 1.3x 10^{-4} g g^{-1}, Böning et al., 2009) and the Gulf of California (1.4 x
607 10^{-4} g g^{-1}, Brumsack, 1989). The deficit between these values and continental crust (2.11 x 10^{-4} g
608 g^{-1}) implies that dissolution of crustal materials along the eastern margin provides a large source
609 of dCo and LCo to the Pacific. In the absence of large hydrothermal inputs (see Section 4.2.5,
610 Swanner et al. 2014), burial of Co depleted sediments on the margin is needed to balance
611 extremely high Co/Al ratios in Pacific pelagic sediments, which collect Co scavenged from the
612 water column (e.g Dunlea et al., 2015; Goldberg and Arrhenius, 1958).
613
614 In contrast to depleted Co along the South American shelf, the Co/Al ratio in shelf sediments
615 from the western margin of the Pacific appears crustal (Table 2). Holocene records from the
616 Pearl River delta and shelf slope in the South China Sea ~20° N (Hu et al., 2012, 2013) show
617 mean Co/Al ratios of 2.2 and 2.1 x 10^{-4} g g^{-1}, respectively, similar to sediments from the Gulf of

Papua at 9° S (2.3 x 10^{-4} g g^{-1}, Alongi et al., 1996). Crustal Co/Al in these sedimentary systems implies that most of the Co provided from fluvial sediment delivery either does not dissolve or is quickly reburied by water column Mn oxidation, rates of which can be very high in estuaries and coastal seas (Moffett and Ho, 1996; Moffett, 1994; Sunda and Huntsman, 1987; Sunda and Huntsman, 1990).

It is likely that oxidizing conditions in the water column and surface sediments limit the release of cobalt on the western margin, leading to crustal Co/Al ratios in shelf sediments, while suboxic conditions on the eastern margin mobilize Co, evident in depleted Co/Al ratios observed there. Although sedimentary anoxia releases Co bound in Mn oxides, even a thin layer of O_2 penetration into sediments results in a near-zero diffusive flux into the water column (Heggie and Lewis, 1984). Indeed, El Niño-driven oxygenation events on the Peru shelf are associated with deposition of Mn-oxides in shallow sediments (Scholz et al. 2011). Bottom water deoxygenation restores Co fluxes to the water column (Johnson et al., 1988, Sundby et al., 1986), but Co is also incorporated into sulfide minerals, analogous to the 'Goldilocks' mechanism for benthic Fe release where flux is maximized when redox conditions are low enough to promote oxide dissolution but still high enough to avoid pyrite burial (into which cobalt is incorporated; Morse and Luther, 1999, Scholz et al., 2014). Cobalt burial in pyrite is evident in high Co/Al content of Black Sea sediments (Brumsack, 2006) and sulfide-rich pockets of Namibian sediments near Walvis Bay (2.9 x 10^{-4} g g^{-1}, Borchers et al., 2005), despite more widespread Co/Al depletion in suboxic (but not sulfidic) terrigenous sediments underneath the Benguela upwelling region (Bremner and Willis, 1993). Prevailing suboxic conditions along the Namibian coast ultimately lead to an extensive dCo plume that reaches across the South Atlantic basin (Noble et al., 2012).

Similarly, depleted sedimentary Co/Al on the Peruvian margin and high dCo in the water column perhaps reflect sustained anoxia that, in the present, is unlikely outside the domain of OMZs.

Altogether, the accumulating evidence that the oceans' major OMZs harbor dCo plumes (Noble et al., 2012, Alhgren et al., 2014, Noble et al., in prep) indicates a strong chemical connection between the efficiency of dCo sources and local redox conditions where these OMZs interact with the continental margin. While reductive dissolution is the most likely mechanism at play, whether this process predominantly occurs in estuaries, the OMZ water column, or margin sediments is presently unclear, but will ultimately dictate how the dCo source (and the resulting OMZ plumes) are affected by climate-driven changes in the size and intensity of OMZs (e.g. Scholz et al. 2011, 2014). As such, there is a significant need for future experimental and field studies that address the redox sensitivity of dCo and other metal fluxes from coastal environments.

4.2.3 Comparing coastal sources with the OMZ cobalt plume

Can a terrigenous cobalt source account for the observed OMZ plume? Because lithogenic sediments along the Peru margin are delivered primarily by rivers (Scheidegger and Krissek, 1982), we can estimate a dCo flux to OMZ waters as the product of the fluvial sediment delivery to the continental shelf and the difference in Co/Al ratios between original rocks and buried shelf sediments:

$$\text{Co flux}_{\text{suboxic}} = \left(\frac{\text{Co}}{\text{Al}}_{\text{crust}} - \frac{\text{Co}}{\text{Al}}_{\text{suboxic sediments}}\right) * \%\,\text{Al} * \text{F}_{\text{fluvial}} \quad (1)$$

where $F_{fluvial}$ is the riverine flux of terrigenous sediments from Ecuador, Peru and Northern Chile to oxygen-depleted coastlines in the ETSP. If this supply is approximately 200 MT year^{-1} (Lyle,

1981; Milliman and Farnsworth, 2011), the Co deficit in Peruvian sediments from Böning et al., 2004 corresponds to a 2.5–4.6 x 10^7 mol per year flux from the South American shelf, depending on the crustal endmember applied (upper continental crust vs. andesite, Table 2). When scaled to the size of the ETSP OMZ (2.2 x 10^6 km^3 defined at 20 μM O_2, Fuenzalida et al., 2009) a terrigenous cobalt supply of 11–21 pM $year^{-1}$ would be expected.

The extent to which the coastal flux and dCo inventory are in agreement depends on the residence time of OMZ waters. Models and CFC distributions from WOCE imply an approximately decadal recirculation time in OMZ waters relative to mesopelagic gyre circulation in the ETSP (Deutsch et al., 2001, 2011). Integrating our terrigenous Co flux estimate over 10 years yields an expected concentration of 120–230 pM within the OMZ. This is of similar magnitude, but greater than the concentrations measured on the GP16 transect (mean of 100 ± 30 pM). The difference between estimated and actual dCo inventories in the OMZ is probably due to upwelling and advection by surface currents, readily seen in the dCo section (Fig. 6), which carries the remainder to the gyre.

4.2.4 Comparison to atmospheric deposition

We can compare the calculated sedimentary flux to an expected flux from aerosol dust dissolution. Aeolian deposition is extremely low over the South Pacific basin (Mahowald et al., 2005), except immediately offshore of Peru, where dust from the Altiplano interacts with the prevailing northward winds (Prospero and Bonatti, 1969; Scheidegger and Krissek, 1982). Model results (Mahowald et al., 2005) suggest that deposition does not exceed 0.5 g m^{-2} yr^{-1}, except very close to the coastline. Using this estimate, crustal cobalt abundances, and the aerial extent of

687 the OMZ (9.8 x 10^6 km^2, Fuenzalida et al., 2009), we estimate the aerial flux of cobalt from dust
688 to be 1.4 x 10^6 mol per year. A 10% fractional solubility for cobalt (Shelley et al., 2012)
689 indicates a soluble cobalt flux from dust of 0.065 pM dCo $year^{-1}$, ~0.5 % of the expected
690 sedimentary flux. Over a decade, dust deposition accounts <1 pM of the OMZ dCo plume. dCo
691 profiles also lack surface maxima near shore despite corresponding features for dissolved Al and
692 Mn at Stations 1 and 5 (Fig. 10, Resing et al., 2015). Fluvial sediment delivery to the margin,
693 therefore, is a much more plausible source for the elevated dCo in the ETSP OMZ.
694
695 **4.2.5 An inefficient cobalt source in hydrothermal vents**
696 Hydrothermal venting along the Eastern Pacific Rise (EPR) provides a major source of dFe and
697 dMn to the deep South Pacific (Resing et al., 2015) where nanomolar concentrations of both
698 metals were measured between 2000–3000 m at the ridge crest and concentrations exceeded
699 background values for several thousand kilometers westward. In contrast, dCo concentrations are
700 only slightly elevated at the ridge crest (Station 18, Fig. 3), reaching 36 pM at 2400m (against a
701 background of ~25 pM); at the same station, dFe and dMn both exceeded 15 nM (background <1
702 nM, Fig. 12a). Unambiguous hydrothermal input is evident from the LCo profile, which peaks at
703 14 pM at the dCo maximum (Fig. 12b), roughly consistent with a 10,000-fold dilution of high
704 temperature endmember sources containing 100–1000 nM dCo (Lupton et al., 1985; Metz and
705 Trefry, 2000).
706
707 However, both dCo and LCo maxima are offset from dFe and dMn plumes. At Station 18, dFe
708 and dMn peak at 2500–2600 m. At this depth, LCo is undetectable and dCo values are at – or
709 slightly lower than – background levels (Fig. 12b), suggesting that Mn and/or Fe scavenging in

the heart of the hydrothermal plume has removed most of the hydrothermal Co from the water column before being transported away from the ridge crest. Indeed, Co is strongly associated with Mn phases in near-axis metalliferous sediment in the EPR at 14° S (Dunk and Mills, 2006). The position of the LCo maximum above the dMn and dFe maxima probably reflects lower scavenging rates outside the main plume, which may spare a fraction of the hydrothermal Co source from an otherwise immediate and total removal. Even without scavenging losses, global hydrothermal Co fluxes (2.2 Mmol $year^{-1}$; Swanner et al., 2014) are 10–25x less than our estimated source from the Peru Shelf alone, highlighting the importance of upper ocean sources in maintaining the dCo inventory.

4.3 Cobalt scarcity in the euphotic zone

4.3.1 The South Pacific Gyre

The combination of eastern boundary upwelling and a continental source produces large dCo gradients across the surface of the South Pacific Ocean (Fig. 6a). Westward, decreasing surface dCo results from phytoplankton uptake and export, reflected in strong correlations with PO_4, as well as mixing with low dCo waters from the subtropical gyre. It is interesting to note that the intercept for the dCo:PO_4 relationship is negative (-12.8 ± 2.6 μM M^{-1}, Fig. 7b); cobalt was depleted before PO_4. This is opposite to what was observed in the Sargasso Sea, where extreme PO_4 scarcity results in a positive dCo:PO_4 intercept (Jakuba et al., 2008). The dCo nutricline in the South Pacific gyre (~200 m, Fig. 6) is also deeper than corresponding features in the North and South Atlantic (Noble et al., 2012; Noble and Saito, in prep). Because winter mixed layers in the tropical South Pacific generally does not exceed 100 m and strong haloclines separate the oxygen minimum layer from the surface (Fiedler and Talley, 2006), convective overturn does not

reach the dCo nutricine at 150–250 m. Low vertical cobalt supply makes the South Pacific gyre an interesting counterpart to the Sargasso Sea, which experiences deep winter mixing and higher dCo (10–30 pM, Dulaquais et al., 2014b; Jakuba et al., 2008; Noble and Saito, in prep), and emphasizes the importance of lateral supply mechanisms, especially eastern boundary upwelling, in maintaining the surface dCo inventory of the tropical Pacific (Saito et al., 2004).

While productivity in the South Pacific is thought to be limited by scarcity of iron and nitrogen (Moore et al., 2013; Saito et al., 2014), the extremely low dCo measured here implies that it may be important as well. Because marine cyanobacteria such as *Prochlorococcus* and *Synechococcus* have an absolute Co requirement (Saito et al., 2002; Sunda and Huntsman, 1995), they are vulnerable to limitation. Indeed, a *Synechococcus* bloom in the Costa Rica Dome was found to be co-limited by both iron and cobalt (Saito et al., 2005). Despite dCo concentrations below 10 pM (sometimes below the 3 pM detection limit), the South Pacific gyre contains a significant *Prochlorococcus* population – evident in the high proportion of divinyl chlorophyll A to total chlorophyll (Fig. 13a). As LCo was undetectable beyond 100° W, biological uptake must occur either by accessing strongly bound dCo or through fast recycling of LCo at very low steady-state concentrations. On GP16, particulate Co concentrations in the upper 50 m were steady (3.5 ± 1.2 pM) and mostly reflect Co bound in biomass (Ohnemus et al., In Press), sometimes rivaling dissolved cobalt concentrations (Fig. 13b). Compared to low pCo:dCo ratios observed in the South Atlantic (<1:12, Noble et al., 2012), the high ratio in the South Pacific gyre (~1:3, Fig. 13b) indicates that resident *Prochlorococcus* are extremely well-adapted to widespread dCo scarcity and that efficient recycling of biogenic pCo may be crucial to survival

of *Prochlorococcus* and other cyanobacteria (e.g. *Synechococcus*, Ahlgren et al. 2014) in the face of widespread dCo scarcity.

4.3.2 Depletion of labile dissolved cobalt in the Peru Upwelling Ecosystem

Unlike its near uniform relationship with dCo in the underlying OMZ, LCo measured on GP16 is low relative to dCo in the surface ocean (0–50 m), especially along the Peru Margin (Figs. 7a, 13c). This might result either from microbial production of cobalt ligands – as observed in a *Synechococcus*-dominated community in the Costa Rica Dome (Saito et al., 2005) and with cultured *Prochlorococcus* strains (Saito et al. 2002) – or if LCo is the preferred species for uptake. The latter has been demonstrated in culture with model eukaryotic algae (Sunda and Huntsman, 1995), where free Co ion is acquired by high affinity Zn-transporters. Because the Peru upwelling region is dominated by diatoms (Bruland et al., 2005), preferential uptake of free Co ion by these organisms is realistic and is corroborated by a strong correlation between LCo and dissolved silicate (Si) in the upper 50 m of the section ($R^2 = 0.90$, Fig. 7c). As a result of diatom-driven export, LCo in shelf surface waters is nearly depleted (1–12 pM) despite high concentrations of dCo (40–80 pM, Fig. 13c). Very low surface LCo at 12° S on GP16 contrasts with previous observations showing high concentrations of LCo in the Peru upwelling region during August–September 2000 (Saito et al., 2004). Between 5–10° S, much higher surface dCo was measured in freshly upwelled waters (up to 315 pM) and dCo was >50 % labile in surface transects (Saito et al., 2004). Surface dFe during August–September 2000 was also higher between 5–10° S than on GP16 at 12° S (Bruland et al., 2005; Resing et al., 2015). Decreasing surface dFe from North to South followed decreasing gradients in shelf width and fluvial sediment supply (Bruland et al., 2005; Milliman and Farnsworth, 2011), implying that the high

dFe was due to stronger benthic sources to the North. Because coastal sources are expected to provide labile cobalt (e.g. Fig 11), the high concentrations of LCo measured between 5–10° S during August–September 2000 indicate a similar gradient in coastal dCo input and LCo availability in surface waters.

Spatial and temporal variability of margin dCo sources may ultimately affect carbon flow through the Peru upwelling ecosystem. Considering the very low dissolved Zn in surface waters on GP16 (<100 pM east of 90° W, S. John personal communication) and that >95 % of the dZn is typically complexed by organic ligands (Bruland, 1989), coastal diatoms in the Peru upwelling region may be subject to diffusion limitation when free Zn ion falls below a 1–10 pM threshold (Sunda and Huntsman, 1992). Because Co can replace Zn in carbonic anhydrase enzymes (Sunda and Huntsman, 1995; Yee and Morel, 1996), LCo supplied from the margin may maintain fast rates of carbon fixation and export in the Peru Upwelling region despite low dZn. The relatively low concentrations measured on GP16, however, imply that the LCo supply may not always be sufficient.

5. Conclusions

A schematic of the cobalt cycle in the Eastern Tropical South Pacific Ocean – and how these processes lead to covariation of dissolved cobalt with O_2 and PO_4 – is shown in Figure 14. High dCo and LCo on the Peru shelf match depleted Co content reported in Peru shelf sediments and indicate a large source to the water column (Böning et al., 2004). Correlations between dMn and LCo in anoxic shelf waters, and crust-like Co/Al ratios in oxic western boundary sediments suggest that margin cobalt sources are redox sensitive and that the sustained presence of the

OMZ on the Peru margin amplifies coastal Co fluxes. The high dCo within the OMZ leads to a large flux to the surface ocean by upwelling along the Peru margin, where it is readily accessed by phytoplankton. The significance of cobalt as a micronutrient is emphasized by strong correlations with phosphate throughout the surface ocean.

The basin scale association between high dCo and low O_2 throughout the GP16 section testifies to the importance of remineralization in maintaining the dCo distribution in the Eastern South Pacific (Fig. 14). Additionally, low oxygen suppresses particulate Mn accumulation and Co scavenging, contributing to the OMZ cobalt plume. Scavenging in oxic mesopelagic waters limits the full return of Co to the dissolved phase during remineralization, resulting in low dissolved Co:P ratios relative to biomass exported from the euphotic zone. Oxidative scavenging also seems to limit the flux of Co from hydrothermal venting over the East Pacific rise, further emphasizing the Peru margin as the most important Co source to the South Pacific. Given that deep nutriclines in the South Pacific Gyre limit dCo supply from vertical mixing outside of the upwelling zone, phytoplankton Co nutrition depends largely on lateral supply from the Eastern Margin.

Ultimately, the dCo inventory in the South Pacific – and its availability to surface phytoplankton – may be changing considerably as the size of the OMZ fluctuates. Recent warming and stratification appear to have expanded the volume of low oxygen waters in the tropics (Stramma et al., 2008, 2010). As such, dCo inventories may increase as lower O_2 hinders mesopelagic Mn oxide production and scavenging. However, decreased wind-driven upwelling and carbon export may cause anoxic waters along the shelf to contract (Deutsch et al., 2011, 2014) and decrease the

efficiency of the coastal dCo source. Changes in the dCo inventory then depend on the relative redox sensitivities of margin Co sources versus offshore scavenging in the mesopelagic, neither of which is well understood. Considering the 100–200 year residence time of Co in the ocean (Saito and Moffett, 2002), feedbacks on the surface dCo supply may manifest more quickly than for other nutrients and may alleviate or exacerbate any existing Co limitation. Improved definition of biological Co limitation thresholds and efforts to reconstruct the Co cycle in past climates may resolve whether future changes in OMZ structure will have meaningful impacts on phytoplankton nutrition in the coming century.

Author Contributions

NJH, DCO and JAR participated on the EPZT cruise. NJH measured dCo and LCo. JAR measured dMn; DCO and BST measured particulate Co, Mn, and P. NJH and MAS prepared the manuscript with contributions from all authors.

Acknowledgements

We thank the Captain and Crew of the RV *Thomas G. Thompson* and the entirety of the science party aboard the GP16 cruise, especially chief scientists Jim Moffett and Chris German. We also thank Claire Parker and Cheryl Zurbrick for enormous efforts in sample collection, Greg Cutter and Geo Smith for operating the trace metal rosette and Tow-Fish, respectively, and Sara Rauschenberg and Rob Sherrell for particle sampling. The Oceanographic Data Facility (ODF) provided nutrient, oxygen, and salinity data and the Bidigare Lab (UH) provided HPLC-pigment analyses. The technical and logistical expertise of Dawn Moran and Matt McIlvin is unparalleled. We appreciate the efforts of the GEOTRACES office in coordinating the GP16

expedition and thank Luca Pini and Mike Kubicsko of Metrohm Autolab for assistance with voltammetry. This is PMEL publication #4475 and JISAO publication 2648. This work was funded by NSF awards OCE-1233733 to MAS, OCE-1232814 to BST, and OCE-1237011 to JAR.

References

Ahlgren, N. A., Noble, A. E., Patton, A. P., Roache-Johnson, K., Jackson, L., Robinson, D., McKay, C., Moore, L. R., Saito, M. A. and Rocap, G.: The unique trace metal and mixed layer conditions of the Costa Rica upwelling dome support a distinct and dense community of Synechococcus, Limnol. Oceanogr., 59(6), 2166–2184, doi:10.4319/lo.2014.59.6.2166, 2014.

Alongi, D. M., Boyle, S. G., Tirendi, F. and Payn, C.: Composition and Behaviour of Trace Metals in Post-oxic Sediments of the Gulf of Papua, Papua New Guinea, Estuar. Coast. Shelf Sci., 42(2), 197–211, doi:10.1006/ecss.1996.0015, 1996.

Baars, O. and Croot, P. L.: Dissolved cobalt speciation and reactivity in the eastern tropical North Atlantic, Mar. Chem., doi:10.1016/j.marchem.2014.10.006, 2015.

Baxter, L. A., Bobrowski, A., Bond, A. M., Heath, G. A, Paul, R. L., Mrzljak, R. and Zarebski, J.: Electrochemical and spectroscopic investigation of the reduction of dimethylglyoxime at mercury electrodes in the presence of cobalt and nickel, Anal. Chem., 70(7), 1312–23, doi:10.1021/ac9703616, 1998.

Biller, D. V. and Bruland, K. W.: Sources and distributions of Mn, Fe, Co, Ni, Cu, Zn, and Cd relative to macronutrients along the central California coast during the spring and summer upwelling season, Mar. Chem., 155, 50–70, doi:10.1016/j.marchem.2013.06.003, 2013.

Böning, P., Brumsack, H. J., Böttcher, M. E., Schnetger, B., Kriete, C., Kallmeyer, J. and Borchers, S. L.: Geochemistry of Peruvian near-surface sediments, Geochim. Cosmochim. Acta, 68(21), 4429–4451, doi:10.1016/j.gca.2004.04.027, 2004.

Böning, P., Brumsack, H. J., Schnetger, B. and Grunwald, M.: Trace element signatures of Chilean upwelling sediments at ~36°S, Mar. Geol., 259(1-4), 112–121, doi:10.1016/j.margeo.2009.01.004, 2009.

Borchers, S. L., Schnetger, B., Böning, P. and Brumsack, H.-J.: Geochemical signatures of the Namibian diatom belt: Perennial upwelling and intermittent anoxia, Geochem., Geophys. Geosyst., 6(6), doi:10.1029/2004GC000886, 2005.

Bown, J., Boye, M., Baker, A., Duvieilbourg, E., Lacan, F., Le Moigne, F., Planchon, F., Speich, S. and Nelson, D. M.: The biogeochemical cycle of dissolved cobalt in the Atlantic and the Southern Ocean south off the coast of South Africa, Mar. Chem., 126(1-4), 193–206, doi:10.1016/j.marchem.2011.03.008, 2011.

Bown, J., Boye, M. and Nelson, D. M.: New insights on the role of organic speciation in the biogeochemical cycle of dissolved cobalt in the southeastern Atlantic and the Southern Ocean, Biogeosciences, 9(7), 2719–2736, doi:10.5194/bg-9-2719-2012, 2012.

Bremner, J. M. and Willis, J. P.: Mineralogy and geochemistry of the clay fraction of sediments from the Namibian continental margin and the adjacent hinterland, Mar. Geol., 115(1-2), 85–116, doi:10.1016/0025-3227(93)90076-8, 1993.

Bruland, K. W.: Complexation of zinc by natural organic ligands in the central North Pacific, Limnol. Oceanogr., 34(2), 269–285, doi:10.4319/lo.1989.34.2.0269, 1989.

Bruland, K. W. and Lohan, M. C.: Controls of Trace Metals in Seawater, Treatise Geochemistry Second Ed., 6, 23–47, doi:10.1016/B978-0-08-095975-7.00602-1, 2003.

Bruland, K. W., Rue, E. L., Smith, G. J. and DiTullio, G. R.: Iron, macronutrients and diatom blooms in the Peru upwelling regime: brown and blue waters of Peru, Mar. Chem., 93(2-4), 81–103, doi:10.1016/j.marchem.2004.06.011, 2005.

Brumsack, H. J.: Geochemistry of recent TOC-rich sediments from the Gulf of California and the Black Sea, Geol. Rundschau, 78(3), 851–882, doi:10.1007/BF01829327, 1989.

Brumsack, H. J.: The trace metal content of recent organic carbon-rich sediments: Implications for Cretaceous black shale formation, Palaeogeogr. Palaeoclimatol. Palaeoecol., 232(2-4), 344–361, doi:10.1016/j.palaeo.2005.05.011, 2006.

Chang, B. X., Devol, A. H. and Emerson, S. R.: Denitrification and the nitrogen gas excess in the eastern tropical South Pacific oxygen deficient zone, Deep Sea Res. Part I Oceanogr. Res. Pap., 57(9), 1092–1101, doi:10.1016/j.dsr.2010.05.009, 2010.

Cowen, J. P. and Bruland, K. W.: Metal deposits associated with bacteria: implications for Fe and Mn marine biogeochemistry, Deep Sea Res. Part A. Oceanogr. Res. Pap., 32(3), 253–272, doi:10.1016/0198-0149(85)90078-0, 1985.

Cutter, G. A. and Bruland, K. W.: Rapid and noncontaminating sampling system for trace elements in global ocean surveys, Limnol. Oceanogr. Methods, 10(6), 425–436, doi:10.4319/lom.2012.10.425, 2012.

Deutsch, C., Gruber, N., Key, R. M., Sarmiento, J. L. and Ganachaud, A.: Denitrification and N2 fixation in the Pacific Ocean, Global Biogeochem. Cycles, 15(2), 483–506, doi:10.1029/2000GB001291, 2001.

Deutsch, C., Brix, H., Ito, T. and Thompson, L.: Climate-forced variability of ocean hypoxia, Science, 333(6040), 336–339, doi:10.1126/science.1202422, 2011.

Deutsch, C., Berelson, W., Thunell, R., Weber, T., Tems, C., McManus, J., Crusius, J., Ito, T., Baumgartner, T., Ferreira, V., Mey, J. and van Geen, A.: Centennial changes in North Pacific anoxia linked to tropical trade winds, Science (80-.)., 345(6197), 665–668, doi:10.1126/science.1252332, 2014.

DeVries, T. and Deutsch, C.: Large-scale variations in the stoichiometry of marine organic matter respiration, Nat. Geosci., 7(November), 1–5, doi:10.1038/ngeo2300, 2014.

DeVries, T., Deutsch, C., Primeau, F., Chang, B. and Devol, A.: Global rates of water-column denitrification derived from nitrogen gas measurements, Nat. Geosci., 5(8), 547–550, doi:10.1038/ngeo1515, 2012.

Dulaquais, G., Boye, M., Middag, R., Owens, S., Puigcorbe, V., Buesseler, K., Masqué, P., de Baar, H. J. W. and Carton, X.: Contrasting biogeochemical cycles of cobalt in the surface western Atlantic Ocean, Global Biogeochem. Cycles, 28(12), 1387–1412, doi:10.1002/2014GB004903, 2014a.

Dulaquais, G., Boye, M., Rijkenberg, M. J. and Carton, X.: Physical and remineralization processes govern the cobalt distribution in the deep western Atlantic Ocean, Biogeosciences, 11(6), 1561–1580, doi:10.5194/bg-11-1561-2014, 2014b.

Dunk, R. M. and Mills, R. A.: The impact of oxic alteration on plume-derived transition metals in ridge flank sediments from the East Pacific Rise, Mar. Geol., 229(3-4), 133–157, doi:10.1016/j.margeo.2006.03.007, 2006.

Dunlea, A. G., Murray, R. W. and Harris, R. N.: Cobalt-based age models of pelagic clay in the South Pacific Gyre, Geochem., Geophys. Geosyst., 16(8), 2964-2710, doi:10.1029/2004GC000886, 2015.

Ellwood, M. J. and van den Berg, C. M.: Determination of organic complexation of cobalt in seawater by cathodic stripping voltammetry, Mar. Chem., 75(1-2), 33–47, doi:10.1016/S0304-4203(01)00024-X, 2001.

Fiedler, P. C. and Talley, L. D.: Hydrography of the eastern tropical Pacific: A review, Prog. Oceanogr., 69(2-4), 143–180, doi:10.1016/j.pocean.2006.03.008, 2006.

Fuenzalida, R., Schneider, W., Garcés-Vargas, J., Bravo, L. and Lange, C.: Vertical and horizontal extension of the oxygen minimum zone in the eastern South Pacific Ocean, Deep Sea Res. Part II Top. Stud. Oceanogr., 56(16), 992–1003, doi:10.1016/j.dsr2.2008.11.001, 2009.

Gaillardet, J., Viers, J. and Dupré, B.: Trace Elements in River Waters, in Treatise on Geochemistry, vol. 5, pp. 225–272, Elsevier., 2003.

Goldberg, E. D. and Arrhenius, G.O.S.: Chemistry of Pacific pelagic sediments, Geochim. Cosmochim. Acta, 13(2), 153–212, doi:10.1016/0016-7037(58)90046-2, 1958.

Heggie, D. and Lewis, T.: Cobalt in pore waters of marine sediments, Nature, 311(5985), 453–455, doi:10.1038/311453a0, 1984.

Hu, D., Böning, P., Köhler, C. M., Hillier, S., Pressling, N., Wan, S., Brumsack, H. J. and Clift, P. D.: Deep sea records of the continental weathering and erosion response to East Asian monsoon intensification since 14ka in the South China Sea, Chem. Geol., 326-327, 1–18, doi:10.1016/j.chemgeo.2012.07.024, 2012.

Hu, D., Clift, P. D., Boning, P., Hannigan, R., Hillier, S., Blusztajn, J., Wan, S. and Fuller, D. Q.: Holocene evolution in weathering and erosion patterns in the Pearl River delta, Geochem., Geophys. Geosyst., 14(7), 2349–2368, doi:10.1002/ggge.20166, 2013.

Jakuba, R. W., Moffett, J. W. and Dyhrman, S. T.: Evidence for the linked biogeochemical cycling of zinc, cobalt, and phosphorus in the western North Atlantic Ocean, Global Biogeochem. Cycles, 22(4), 1–13, doi:10.1029/2007GB003119, 2008.

Johnson, K. S., Stout, P. M., Berelson, W. M. and Sakamoto-Arnold, C. M.: Cobalt and copper distributions in the waters of Santa Monica Basin, California, Nature, 332(6164), 527–530, doi:10.1038/332527a0, 1988.

Johnson, K. S., Coale, K. H., Berelson, W. M. and Michael Gordon, R.: On the formation of the

manganese maximum in the oxygen minimum, Geochim. Cosmochim. Acta, 60(8), 1291–1299, doi:10.1016/0016-7037(96)00005-1, 1996.

Karstensen, J., Stramma, L. and Visbeck, M.: Oxygen minimum zones in the eastern tropical Atlantic and Pacific oceans, Prog. Oceanogr., 77(4), 331–350, doi:10.1016/j.pocean.2007.05.009, 2008.

Knauer, G. A., Martin, J. H. and Gordon, R. M.: Cobalt in north-east Pacific waters, Nature, 297(5861), 49–51, doi:10.1038/297049a0, 1982.

von Langen, P. J., Johnson, K. S., Coale, K. H. and Elrod, V. A.: Oxidation kinetics of manganese (II) in seawater at nanomolar concentrations, Geochim. Cosmochim. Acta, 61(23), 4945–4954, doi:10.1016/S0016-7037(97)00355-4, 1997.

Lupton, J. E., Delaney, J. R., Johnson, H. P. and Tivey, M. K.: Entrainment and vertical transport of deep-ocean water by buoyant hydrothermal plumes, Nature, 316(6029), 621–623, doi:10.1038/316621a0, 1985.

Lyle, M.: Formation and growth of ferromanganese oxides on the Nazca plate, Geological Society of America Memoirs, 154, 269–295, doi:10.1130/MEM154-p269, 1981.

Mahowald, N. M., Baker, A. R., Bergametti, G., Brooks, N., Duce, R. a., Jickells, T. D., Kubilay, N., Prospero, J. M. and Tegen, I.: Atmospheric global dust cycle and iron inputs to the ocean, Global Biogeochem. Cycles, 19(4), doi:10.1029/2004GB002402, 2005.

McLennan, S. M.: Relationships between the trace element composition of sedimentary rocks and upper continental crust, Geochem., Geophys. Geosyst., 2(4), doi:10.1029/2000GC000109, 2001.

Metz, S. and Trefry, J. H.: Chemical and mineralogical influences on concentrations of trace metals in hydrothermal fluids, Geochim. Cosmochim. Acta, 64(13), 2267–2279, doi:10.1016/S0016-7037(00)00354-9, 2000.

Milliman, J. D. and Farnsworth, K. L.: River Discharge to the Coastal Ocean, Cambridge University Press, Cambridge., 2011.

Moffett, J. W.: A radiotracer study of cerium and manganese uptake onto suspended particles in Chesapeake Bay, Geochim. Cosmochim. Acta, 58(2), 695–703, doi:10.1016/0016-7037(94)90499-5, 1994.

Moffett, J. W. and Ho, J.: Oxidation of cobalt and manganese in seawater via a common microbially catalyzed pathway, Geochim. Cosmochim. Acta, 60(18), 3415–3424, doi:10.1016/0016-7037(96)00176-7, 1996.

Moore, C. M., Mills, M. M., Arrigo, K. R., Berman-Frank, I., Bopp, L., Boyd, P. W., Galbraith, E. D., Geider, R. J., Guieu, C., Jaccard, S. L., Jickells, T. D., La Roche, J., Lenton, T. M., Mahowald, N. M., Marañón, E., Marinov, I., Moore, J. K., Nakatsuka, T., Oschlies, A., Saito, M. A, Thingstad, T. F., Tsuda, A. and Ulloa, O.: Processes and patterns of oceanic nutrient limitation, Nat. Geosci., 6(9), 701–710, doi:10.1038/ngeo1765, 2013.

Morse, J. W. and Luther, G. W.: Chemical influence on trace metal-sulfide interactions in anoxic sediments, Geochim. Cosmochim. Acta, 63(3373–3378), 3378, 1999.

Noble, A. E. and Saito, M. A.: Total Dissolved Cobalt and Cobalt Speciation from the US North Atlantic GEOTRACES Zonal Transect, in prep.

Noble, A. E., Saito, M. A., Maiti, K. and Benitez-Nelson, C. R.: Cobalt, manganese, and iron near the Hawaiian Islands: A potential concentrating mechanism for cobalt within a cyclonic eddy and implications for the hybrid-type trace metals, Deep Sea Res. Part II Top. Stud. Oceanogr., 55(10-13), 1473–1490, doi:10.1016/j.dsr2.2008.02.010, 2008.

Noble, A. E., Lamborg, C. H., Ohnemus, D. C., Lam, P. J., Goepfert, T. J., Measures, C. I., Frame, C. H., Casciotti, K. L., DiTullio, G. R., Jennings, J. and Saito, M. A.: Basin-scale inputs of cobalt, iron, and manganese from the Benguela-Angola front to the South Atlantic Ocean, Limnol. Oceanogr., 57(4), 989–1010, doi:10.4319/lo.2012.57.4.0989, 2012.

Ohnemus, D., Rauschenberg, S., Cutter, G. A. and Twining, B. S.: Elevated trace metal content of prokaryotic plankton communities associated with anoxic marine zones. Limnol. Oceanogr., doi:10.1002/lno.10363, In Press.

Price, N. M., Harrison, G. I., Hering, J. G., Hudson, R. J., Nirel, P. M. V., Palenik, B. and Morel, F. M. M.: Preparation and Chemistry of the Artificial Algal Culture Medium Aquil, Biol. Oceanogr., 6(5-6), 443–461, doi:10.1080/01965581.1988.10749544, 1989.

Prospero, J. M. and Bonatti, E.: Continental dust in the atmosphere of the Eastern Equatorial Pacific, J. Geophys. Res., 74(13), 3362–3371, doi:10.1029/JC074i013p03362, 1969.

Resing, J. A., Sedwick, P. N., German, C. R., Jenkins, W. J., Moffett, J. W., Sohst, B. M. and Tagliabue, A.: Basin-scale transport of hydrothermal dissolved metals across the South Pacific Ocean, Nature, 523(7559), 200–203, doi:10.1038/nature14577, 2015.

Saito, M. A. and Moffett, J. W.: Complexation of cobalt by natural organic ligands in the Sargasso Sea as determined by a new high-sensitivity electrochemical cobalt speciation method suitable for open ocean work, Mar. Chem., 75(1-2), 49–68, doi:10.1016/S0304-4203(01)00025-1, 2001.

Saito, M. A. and Moffett, J. W.: Temporal and spatial variability of cobalt in the Atlantic Ocean, Geochim. Cosmochim. Acta, 66(11), 1943–1953, doi:10.1016/S0016-7037(02)00829-3, 2002.

Saito, M. A., Moffett, J. W., Chisholm, S. W. and Waterbury, J. B.: Cobalt limitation and uptake in Prochlorococcus, Limnol. Oceanogr., 47(6), 1629–1636, doi:10.4319/lo.2002.47.6.1629, 2002.

Saito, M. A., Moffett, J. W. and DiTullio, G. R.: Cobalt and nickel in the Peru upwelling region: A major flux of labile cobalt utilized as a micronutrient, Global Biogeochem. Cycles, 18(4), doi:10.1029/2003GB002216, 2004.

Saito, M. A., Rocap, G. and Moffett, J. W.: Production of cobalt binding ligands in a Synechococcus feature at the Costa Rica upwelling dome, Limnol. Oceanogr., 50(1), 279–290, doi:10.4319/lo.2005.50.1.0279, 2005.

Saito, M. A., Goepfert, T. J., Noble, A. E., Bertrand, E. M., Sedwick, P. N. and DiTullio, G. R.: A seasonal study of dissolved cobalt in the Ross Sea, Antarctica: micronutrient behavior, absence of scavenging, and relationships with Zn, Cd, and P, Biogeosciences, 7(12), 4059–4082, doi:10.5194/bg-7-4059-2010, 2010.

Saito, M. A., McIlvin, M. R., Moran, D. M., Goepfert, T. J., DiTullio, G. R., Post, A. F. and Lamborg, C. H.: Multiple nutrient stresses at intersecting Pacific Ocean biomes detected by protein biomarkers, Science, 345(6201), 1173–1177, doi:10.1126/science.1256450, 2014.

Sarmiento, J. L., Gruber, N., Brzezinski, M. A. and Dunne, J. P.: High-latitude controls of

thermocline nutrients and low latitude biological productivity, Nature, 479(7374), 556–556, doi:10.1038/nature10605, 2011.

Scheidegger, K. F. and Krissek, L. A.: Dispersal and deposition of eolian and fluvial sediments off Peru and northern Chile, Geol. Soc. Am. Bull., 93(2), 150, doi:10.1130/0016-7606(1982)93<150:DADOEA>2.0.CO;2, 1982.

Scholz, F., Hensen, C., Noffke, A., Rohde, A., Liebetrau, V. and Wallmann, K.: Early diagenesis of redox-sensitive trace metals in the Peru upwelling area - response to ENSO-related oxygen fluctuations in the water column, Geochim. Cosmochim. Acta, 75(22), 7257–7276, doi:10.1016/j.gca.2011.08.007, 2011.

Scholz, F., McManus, J., Mix, A. C., Hensen, C. and Schneider, R. R.: The impact of ocean deoxygenation on iron release from continental margin sediments, Nat. Geosci., 7(May), 433–437, doi:10.1038/ngeo2162, 2014.

Shaked, Y., Xu, Y., Leblanc, K. and Morel, F. M. M.: Zinc availability and alkaline phosphatase activity in Emiliania huxleyi: Implications for Zn-P co-limitation in the ocean, Limnol. Oceanogr., 51(1), 299–309, doi:10.4319/lo.2006.51.1.0299, 2006.

Shelley, R. U., Sedwick, P. N., Bibby, T. S., Cabedo-Sanz, P., Church, T. M., Johnson, R. J., Macey, A. I., Marsay, C. M., Sholkovitz, E. R., Ussher, S. J., Worsfold, P. J. and Lohan, M. C.: Controls on dissolved cobalt in surface waters of the Sargasso Sea: Comparisons with iron and aluminum, Global Biogeochem. Cycles, 26(2), doi:10.1029/2011GB004155, 2012.

Sholkovitz, E. R. and Copland, D.: The coagulation, solubility and adsorption properties of Fe, Mn, Cu, Ni, Cd, Co and humic acids in a river water, Geochim. Cosmochim. Acta, 45(2), 181–189, doi:10.1016/0016-7037(81)90161-7, 1981.

Slemons, L. O., Murray, J. W., Resing, J., Paul, B. and Dutrieux, P.: Western Pacific coastal sources of iron, manganese, and aluminum to the Equatorial Undercurrent, Global Biogeochem. Cycles, 24(3), doi:10.1029/2009GB003693, 2010.

Stramma, L., Johnson, G. C., Sprintall, J. and Mohrholz, V.: Expanding Oxygen-Minimum Zones in the Tropical Oceans, Science, 320(5876), 655–658, doi:10.1126/science.1153847, 2008.

Stramma, L., Johnson, G. C., Firing, E. and Schmidtko, S.: Eastern Pacific oxygen minimum zones: Supply paths and multidecadal changes, J. Geophys. Res., 115(C9), C09011, doi:10.1029/2009JC005976, 2010.

Sunda, W. G. and Huntsman, S. A.: Diel cycles in microbial manganese oxidation and manganese redox speciation in coastal waters of the Bahama Islands, Limnol. Oceanogr., 35(2), 325–338, doi:10.4319/lo.1990.35.2.0325, 1990.

Sunda, W. G. and Huntsman, S. A.: Microbial oxidation of manganese in a North Carolina estuary, Limnol. Oceanogr., 32(3), 552–564, doi:10.4319/lo.1987.32.3.0552, 1987.

Sunda, W. G. and Huntsman, S. A.: Feedback interactions between zinc and phytoplankton in seawater, Limnol. Oceanogr., 37(1), 25–40, doi:10.4319/lo.1992.37.1.0025, 1992.

Sunda, W. G. and Huntsman, S. A.: Cobalt and zinc interreplacement in marine phytoplankton: biological and geochemical implications, Limnol. Oceanogr., 40(8), 1404–1417, doi:10.4319/lo.1995.40.8.1404, 1995.

Sundby, B., Anderson, L. G., Hall, P. O. J., Iverfeldt, Å., van der Loeff, M. M. R. and Westerlund, S. F. G.: The effect of oxygen on release and uptake of cobalt, manganese, iron and phosphate at the sediment-water interface, Geochim. Cosmochim. Acta, 50(6), 1281–1288, doi:10.1016/0016-7037(86)90411-4, 1986.

Swanner, E. D., Planavsky, N. J., Lalonde, S. V., Robbins, L. J., Bekker, A., Rouxel, O. J., Saito, M. A., Kappler, A., Mojzsis, S. J. and Konhauser, K. O.: Cobalt and marine redox evolution, Earth Planet. Sci. Lett., 390, 253–263, doi:10.1016/j.epsl.2014.01.001, 2014.

Taylor, S. R. and McLennan, S. M.: The geochemical evolution of the continental crust, Rev. Geophys., 33(2), 241, doi:10.1029/95RG00262, 1995.

Toggweiler, J. R., Dixon, K. and Broecker, W. S.: The Peru upwelling and the ventilation of the South Pacific thermocline, J. Geophys. Res., 96(C11), 20467, doi:10.1029/91JC02063, 1991.

Tovar-Sánchez, A., Sañudo-Wilhelmy, S. A. and Flegal, A. R.: Temporal and spatial variations in the biogeochemical cycling of cobalt in two urban estuaries: Hudson River Estuary and San Francisco Bay, Estuar. Coast. Shelf Sci., 60(4), 717–728, doi:10.1016/j.ecss.2004.03.010, 2004.

Twining, B. S. and Baines, S. B.: The Trace Metal Composition of Marine Phytoplankton, Ann. Rev. Mar. Sci., 5(1), 191–215, doi:10.1146/annurev-marine-121211-172322, 2013.

Ulloa, O., Canfield, D. E., DeLong, E. F., Letelier, R. M. and Stewart, F. J.: Microbial oceanography of anoxic oxygen minimum zones., Proc. Natl. Acad. Sci. U. S. A., 109(40), 15996–6003, doi:10.1073/pnas.1205009109, 2012.

Yee, D. and Morel, F. M. M.: In vivo substitution of zinc by cobalt in carbonic anhydrase of a marine diatom, Limnol. Oceanogr., 41(3), 573–577, doi:10.4319/lo.1996.41.3.0573, 1996.

Table 1. Blanks and standards used during analyses.

		dCo, pM	+/-	n	Consensus
At sea	Blank	3.7	1.2	28	
Oct – Dec,	Lab SW*	4.5	2.1	28	
2013	D1	48.5	2.4	3	46.6 +/- 4.8
At WHOI,	Blank	4.7	1.4	12	
Sept – Nov,	GSP	2.5	2.0	10	4.9 +/-
2014					1.2**
	D2	45.0	2.7	7	46.9 +/- 3.0
	GSC	77.7	2.4	4	***

* South Pacific surface seawater, collected Nov. 2011

**Refers to SAFe standard S, collected at the same location as GSP

***No consensus

Table 2. Co/Al ratios in sediments from different redox regimes.

Location	Co/Al x 10^{-4} (g g^{-1})		Reference
Crust			
Upper continental crust	2.11		McLennan 2001
Andesitic crust	2.63		Taylor and McLennan 1995
Eastern Boundary sediments			
Peru Upwelling Sediments	1.2 ± 0.3	9–14° S	Boning et al. 2004
Chile upwelling Sediments	1.3 ± 0.1	36° S	Boning et al. 2009
Gulf of California	1.4	22–30° N	Brumsack 1989
Namibian Shelf	1.0 ± 0.3	17–25° S, 'Terrigenous'	Bremner and Willis 1993
Sulfidic Sediments			
Namibian diatom belt	2.9 ± 0.7	Near Walvis Bay, 22.5° S	Borchers et al. 2005
Black Sea	3.8–6.2		Brumsack 2006
Western Boundary Sediments			
Papua New Guinea	2.3	8° S, Gulf of Papua	Alongi et al. 1996
Pearl River Delta	2.2 ± 0.4	22° N, (10–0 ka)	Hu et al. 2013
South China Sea Shelf Slope	2.1 ± 0.2	20° N, 2037m (14–0 ka)	Hu et al. 2012
Deep Ocean Sediments			
South Pacific Gyre	35 (2.9–101)	22° S–32° S, 100–0 Ma	Dunlea et al. 2015
Pelagic Pacific	17 (2–58)	50° N–20° S	Goldberg and Arrhenius 1958

Figure Captions

Figure 1. The GP16 transect in the tropical South Pacific. Red circles indicate sampling stations. Dissolved oxygen at a depth of 300 m from the WOCE dataset is plotted in blue and 10 μM contours are shown between 0–60 μM O_2. Station number increases sequentially westward, with the exception of Station 1.

Figure 2. Signal processing of voltammetry scans. Varying instrumental noise imprinted negative current excursions during measurement and necessitated data smoothing to correctly measure the $Co(DMG)_2$ reduction peak at -1.15 V. For mild (a) and moderate (b) noise levels, a 2^{nd} order, 17-point smoothing was applied (red line, 97 % of scans). Increases in noise caused this routine to overestimate peak height (c, red line) and a first order, 13-point smoothing was applied instead (~3 % of scans, blue line).

Figure 3. Profiles of dissolved cobalt (dCo, closed circles), labile dissolved cobalt (LCo, open circles) and O_2 (grey lines) across the South Pacific. Upper panels show a 0–1000 m depth range; bottom panel show full profiles. dCo and LCo are highest close to the Peru Margin (Station 1) and decrease westward. O_2 follows the opposite trend. The small peak at 2400 m at Station 18 shows peak hydrothermal input from the East Pacific Rise. Note that the dCo and LCo scales in the upper panel are adjusted to highlight gradients and differ from the lower panels.

Figure 4. Dissolved oxygen (a), dissolved cobalt (b) and labile dissolved cobalt (c) sections along GP16, projected on a longitudinal axis. Note high dCo and LCo stem from the Peru margin and overlap with the low O_2. Interpolations were made using Ocean Data View with DIVA gridding, with negative gridded values suppressed. The signal to noise ratio was set to 15 for dissolved cobalt and labile dissolved cobalt. Signal to noise for O_2 was set to the default, 50.

Figure 5. Coupling between dissolved cobalt with O_2 (a), AOU (b), and PO_4 (c). Below 200 m (red circles), dCo shows a decreasing linear trend with dissolved oxygen that is obscured upon conversion of O_2 to apparent oxygen utilization, AOU, and a weak relationship with PO_4. In the surface ocean (0–50 m, cyan circles), dCo and PO_4 are strongly coupled but dCo shows no relationship with O_2 or AOU. Samples from 50–200 m are plotted in blue. Trend lines in (c) show least-squares regressions of dCo and PO_4. (0–50 m, cyan; 50–200 m, blue; 200–1000 m, red). Also plotted is the median particulate Co:P ratio for 0–50 m (146 μM M^{-1}, dotted line). Major processes affecting these plots are described in vector legends.

Figure 6. Dissolved cobalt (a), labile dissolved cobalt (b), and particulate cobalt (c) gradients in the upper 500 m of the ETSP. White lines in both panels show dissolved PO_4 contours at 0.5 μM increments. Interpolation was conducted using weight averaged gridding with 40 and 46 ‰ length scales in the x and y directions, respectively.

Figure 7. (a) The relationship between dissolved cobalt (dCo) and labile cobalt (LCo) in the South Pacific. LCo increases linearly with dCo with a slope of 0.33 (black dots, $R^2 = 0.88$), except for the upper 50 m (red dots), where samples fall below this trend due to preferential depletion of LCo by phytoplankton. (b) In the 0–50 m range, dCo strongly correlates with phosphate ($R^2 = 0.89$). (c) LCo is preferentially removed from surface waters (0–50 m) and tracks silicate ($R^2 = 0.90$).

Figure 8. Transition in dCo cycling at the OMZ boundary in the upper South Pacific thermocline. (a) Isopycnal windows centered at $\sigma_\theta = 26.2 \pm 0.1$ kg m^{-3} (circles) and $\sigma_\theta = 26.4 \pm 0.1$ kg m^{-3} (triangles) show PO_4-coupled cycling in oxygenated waters (blue) but not in OMZ waters with <20 μM O_2 (red). (b) In the OMZ, dCo follows salinity, indicating mixing between a high dCo endmember at a salinity of 35.0 and a fresher water mass that is low in dCo.

Figure 9. Redox control of Co and Mn scavenging. Within mesopelagic waters ($\sigma_\theta = 26.2–27.0$ kg m^{-3}, mean depth of 300 m), high O_2 in ventilating water masses result in a sharp redox boundary at the edge of the OMZ (red circles, scale in μM). Particulate Mn (pMn) increases across the oxic/anoxic boundary at 100° W (blue circles, in nM) and imply stabilization of Mn oxides. Both pMn:pP and pCo:pP (cyan and pink circles, respectively; units are M M^{-1}) increase

1179 across the OMZ boundary, exceeding predicted values from remineralization of biogenic
1180 material from the surface ocean (1.26 x 10^{-3} mean pMn:pP and 1.57 x 10^{-4} pCo:pP for 0–50 m
1181 (M M^{-1}), cyan and pink lines, respectively). Dissolved phase dCo:dPO_4 (black circles) and
1182 LCo:PO_4 (white circles) also decrease west of the OMZ boundary show scavenging of the dCo
1183 and LCo in the mesopelagic (units are M M^{-1}).
1184
1185 **Figure 10.** Profiles of dissolved cobalt (dCo, black), PO_4 (red) and dMn (blue) over the Peru
1186 shelf at 12° S. The oxycline (grey bar, defined by the first sample where O_2 <10 μM) marks the
1187 transition between the OMZ and oxygenated surface waters. Station 2 is the closest to the coast.
1188 Note the similarity between dCo and PO_4 above the oxycline and the transition to a dMn-like
1189 profile beneath.
1190
1191 **Figure 11.** Cobalt and Mn in the Peru shelf OMZ (GP16 Stations 1–5, O_2 <20 uM). Dissolved
1192 cobalt (dCo, closed circled) and labile cobalt (LCo, white) follow positive linear relationships
1193 with dMn. The LCo slope (18 mM M^{-1}) approximates the Co:Mn ratio in upper continental crust
1194 and Andesite (red and pink lines 21 and 26 mM M^{-1}, respectively), suggesting it derives from a
1195 crustal source. The mean pCo:pMn ratio from phytoplankton dominated particles collected in the
1196 upper 40 m over the shelf (blue line, 105 mM M^{-1}) is greater than dCo:dMn slope (42 mM M^{-1}),
1197 indicating that dCo and dMn concentrations in the Peru shelf OMZ represent a combination of
1198 biomass remineralization and sedimentary input.
1199
1200 **Figure 12.** Profiles from Station 18 at the East Pacific Rise ridge crest at 113 °W, 15 °S. (a) dMn
1201 (blue lines) and dFe profiles (red) replotted from Resing et al. 2015 clearly show hydrothermal

input. Grey shading below 2250 m indicates area of hydrothermal influence where dFe and dMn are >1 nM. (b) Dissolved cobalt (dCo, black circles) and labile cobalt (LCo, white) in the East Pacific Rise hydrothermal plume.

Figure 13. (a) The ratio of divinyl chlorophyll A to total chlorophyll (green circles), an indication of *Prochlorococcus* abundance relative to other phytoplankton. (b) The particulate to dissolved ratio of cobalt (pCo:dCo, in M M^{-1}, pink circles) in near-surface samples (0–50m) measured on GP16; a value of 1 indicates equal concentrations in each phase. (c) The near-surface distribution of dissolved cobalt (dCo, black circles) and labile cobalt (LCo, white circles), showing higher concentrations near the Peru margin (<80° W) and very low dCo to the west.

Figure 14. Schematic cross-section of the cobalt cycle in the Eastern Tropical South Pacific. Black arrows describe idealized physical circulation, showing upwelling near the Peru margin, advection westward and subduction in the South Pacific gyre. Biological Co export is shown in the red-hashed arrows, and solid and dashed red arrows show remineralization and scavenging respectively. The margin source is shown as a red-outlined arrow. These vectors are also plotted on idealized oxygen and phosphate axes, using the same color scheme, to show how these processes appear in Co:O_2 and Co:PO_4 space.

Figure 1

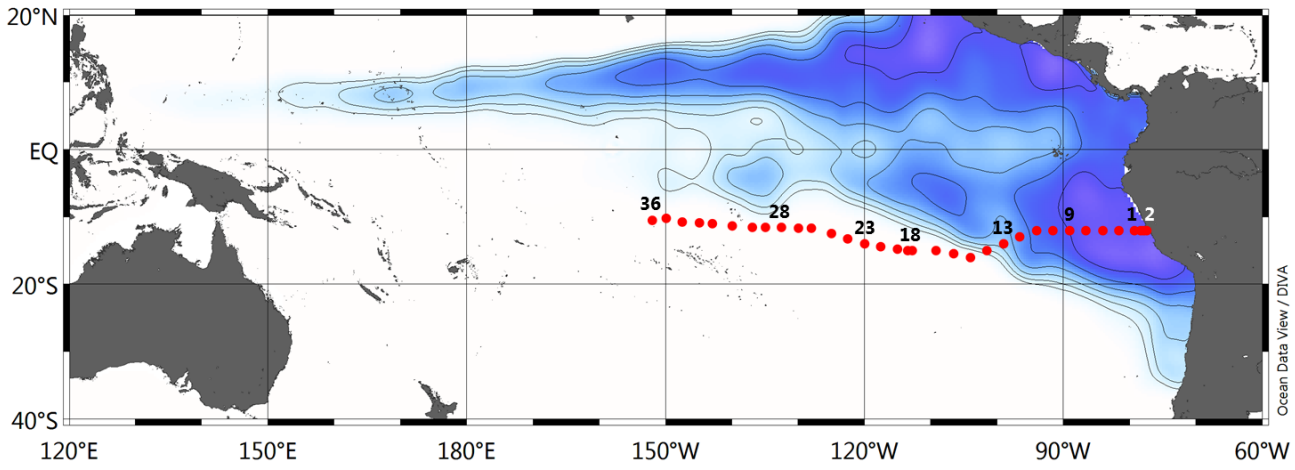
20°N
EQ
20°S
40°S
120°E
150°E
180°E
150°W
120°W
90°W
60°W
36
28
23
18
13
9
1
2
Ocean Data View / DIVA

Figure 2

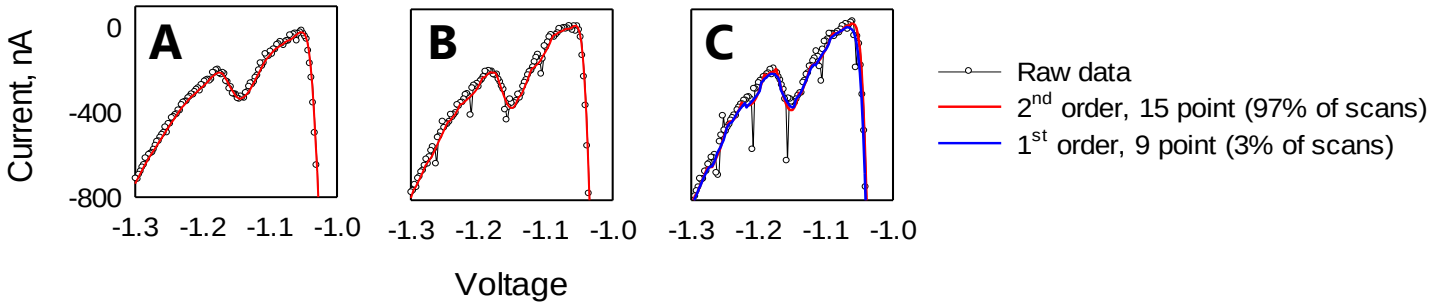
Current, nA
0
-400
-800
A
B
C
-1.3
-1.2
-1.1
-1.0
Voltage
Raw data
2nd order, 15 point (97% of scans)
1st order, 9 point (3% of scans)

Figure 3

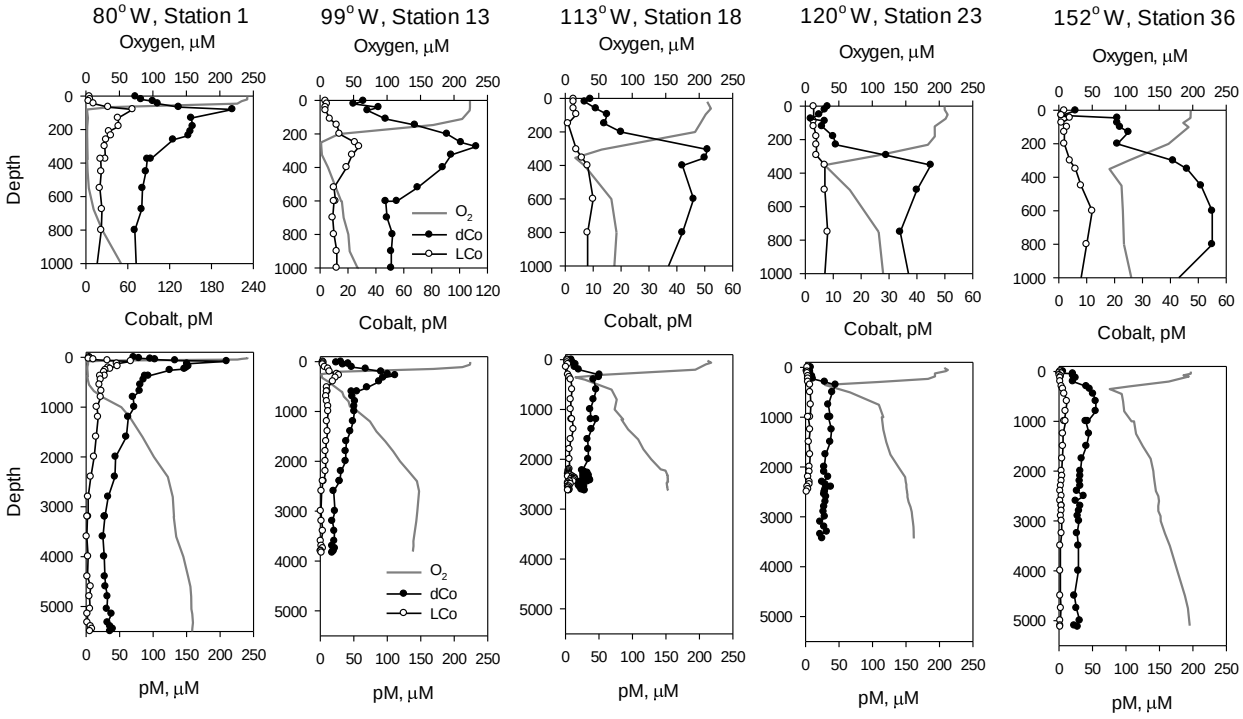
80° W, Station 1
99° W, Station 13
113° W, Station 18
120° W, Station 23
152° W, Station 36
Oxygen, μM
Depth
Cobalt, pM
pM, μM
O2
dCo
LCo

Figure 4

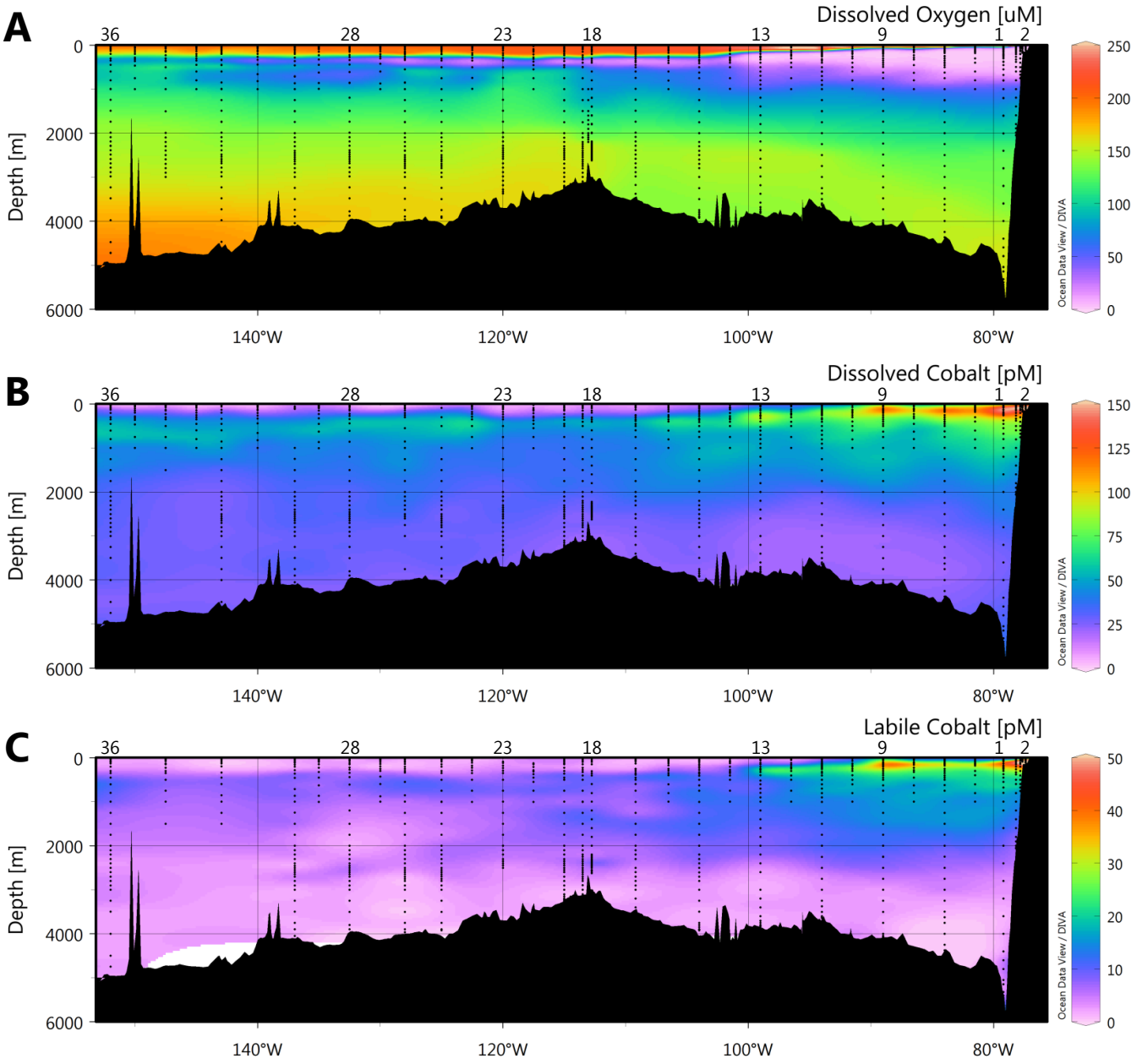
A
Dissolved Oxygen [uM]
36
28
23
18
13
9
1
2
0
2000
4000
6000
Depth [m]
140°W
120°W
100°W
80°W
250
200
150
100
50
0
Ocean Data View / DIVA
B
Dissolved Cobalt [pM]
150
125
100
75
50
25
C
Labile Cobalt [pM]
40
30
20
10

Figure 5

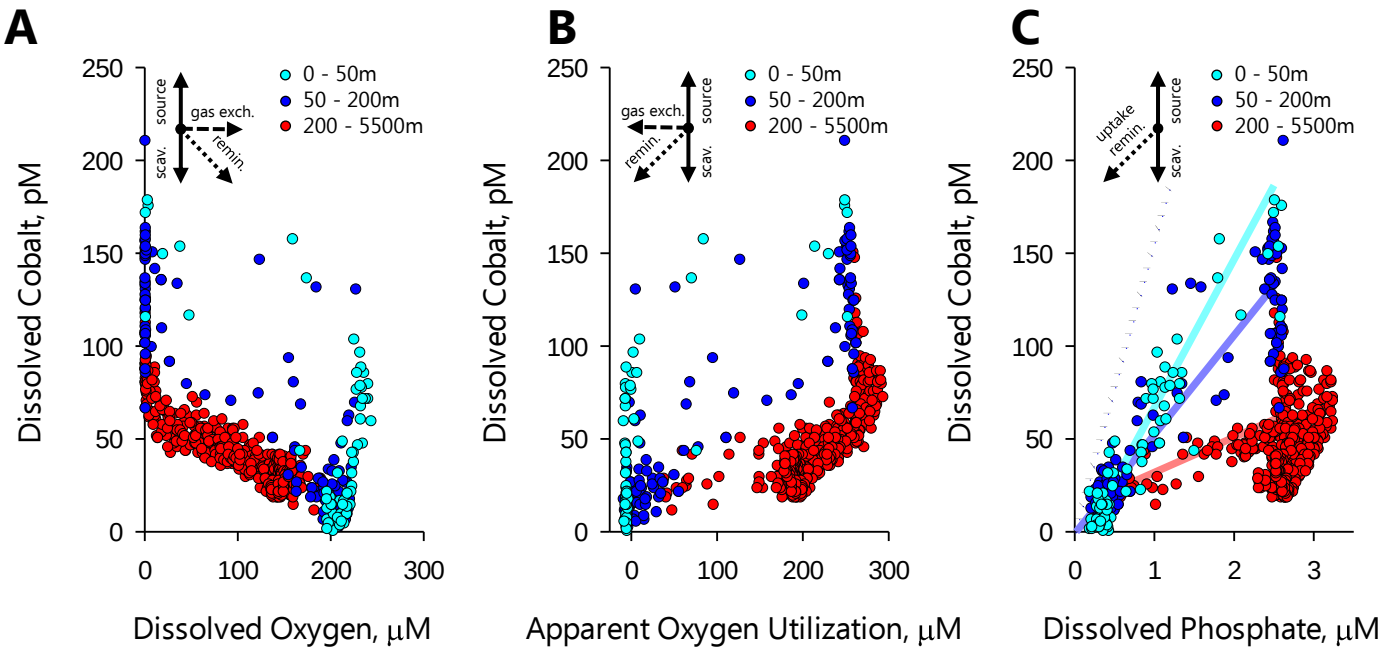
A
B
C
Dissolved Cobalt, pM
Dissolved Oxygen, μM
Apparent Oxygen Utilization, μM
Dissolved Phosphate, μM
0 - 50m
50 - 200m
200 - 5500m
gas exch.
remin.
source
scav.
uptake
0
50
100
150
200
250
0
100
200
300
1
2
3

Figure 6

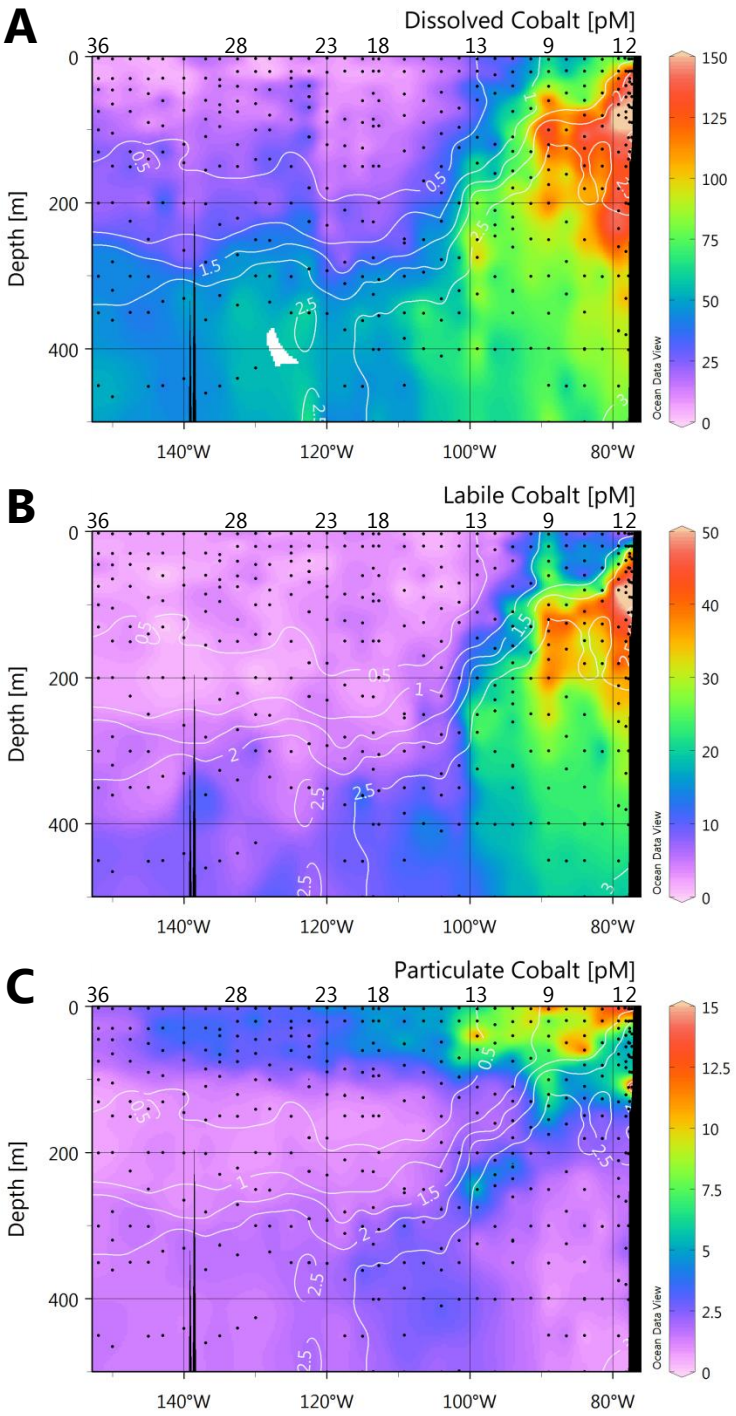
A
Dissolved Cobalt [pM]
B
Labile Cobalt [pM]
C
Particulate Cobalt [pM]
36
28
23
18
13
9
12
0
200
400
Depth [m]
140°W
120°W
100°W
80°W
Ocean Data View

Figure 7

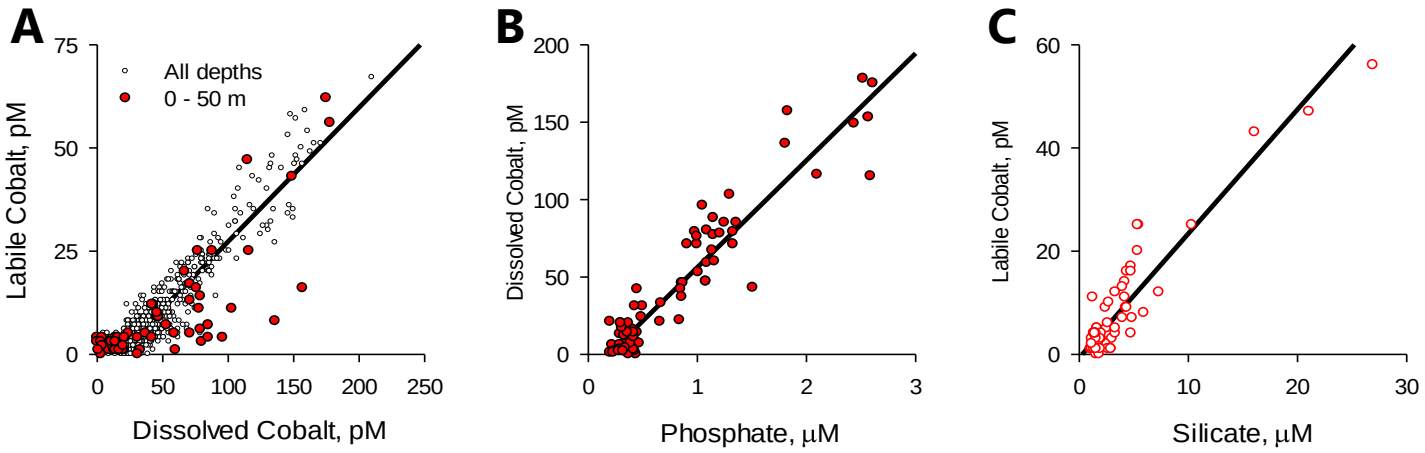
A
All depths
0 - 50 m
Labile Cobalt, pM
Dissolved Cobalt, pM
0
25
50
75
0
50
100
150
200
250
B
Dissolved Cobalt, pM
Phosphate, µM
0
50
100
150
200
0
1
2
3
C
Labile Cobalt, pM
Silicate, µM
0
20
40
60
0
10
20
30

Figure 8

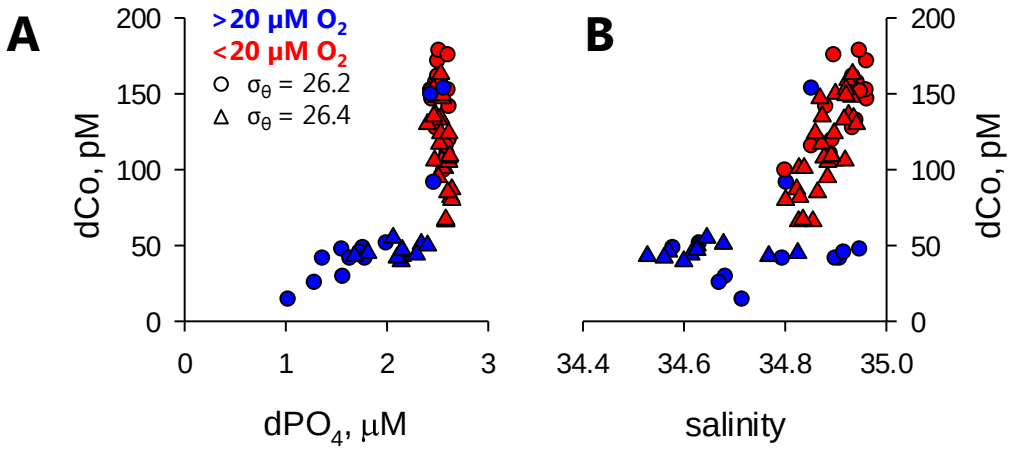

Figure 9

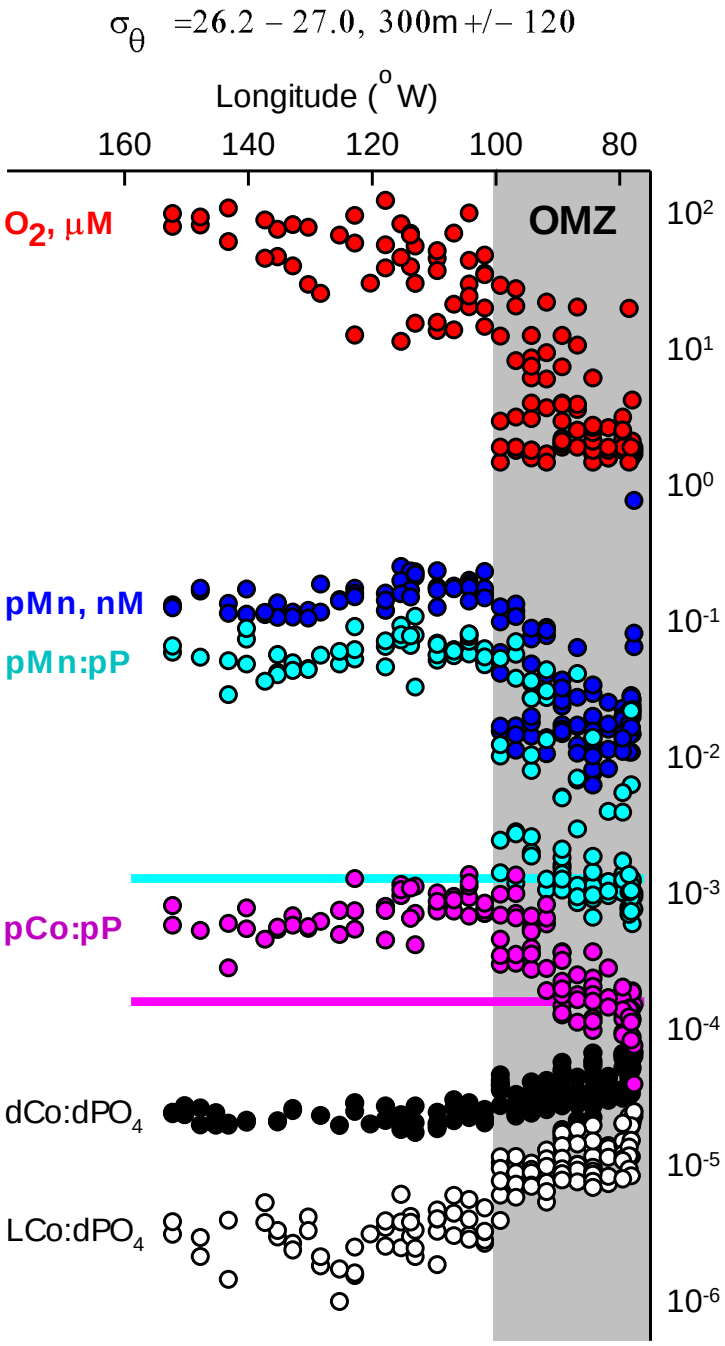
σθ =26.2 – 27.0, 300m +/– 120
Longitude (°W)
160
140
120
100
80
O2, µM
OMZ
pMn, nM
pMn:pP
pCo:pP
dCo:dPO4
LCo:dPO4
10^2
10^1
10^0
10^-1
10^-2
10^-3
10^-4
10^-5
10^-6

Figure 10

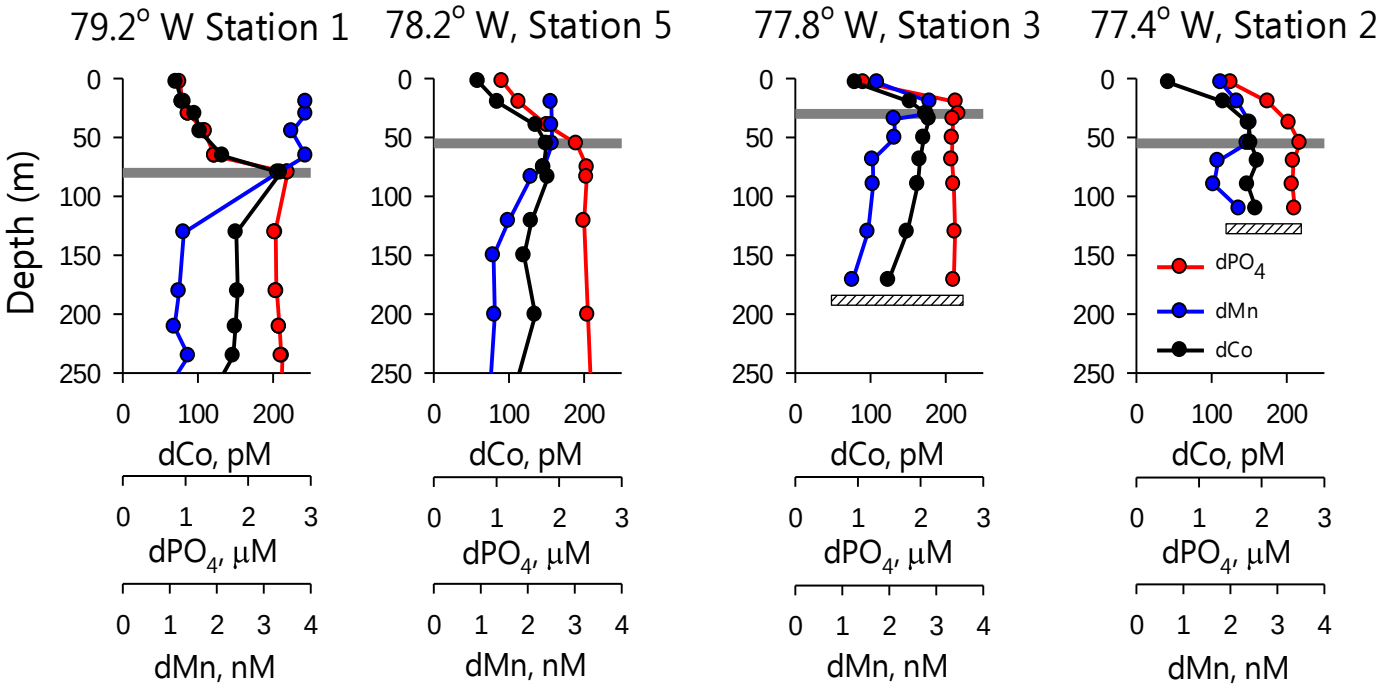
79.2° W Station 1
78.2° W, Station 5
77.8° W, Station 3
77.4° W, Station 2
Depth (m)
0
50
100
150
200
250
dCo, pM
0
100
200
dPO4, µM
0
1
2
3
dMn, nM
0
1
2
3
4
dPO4
dMn
dCo

Figure 11

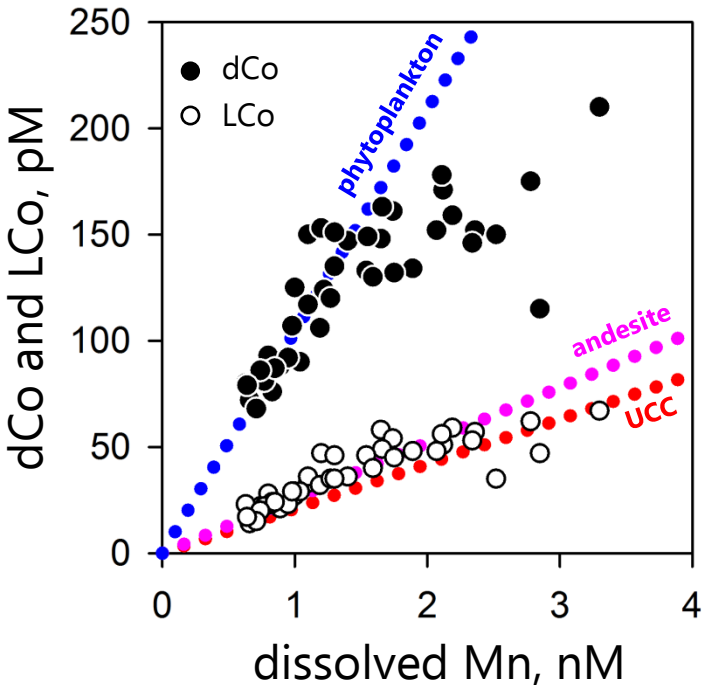
250
200
150
100
50
0
dCo and LCo, pM
dCo
LCo
phytoplankton
andesite
UCC
0
1
2
3
4
dissolved Mn, nM

Figure 12

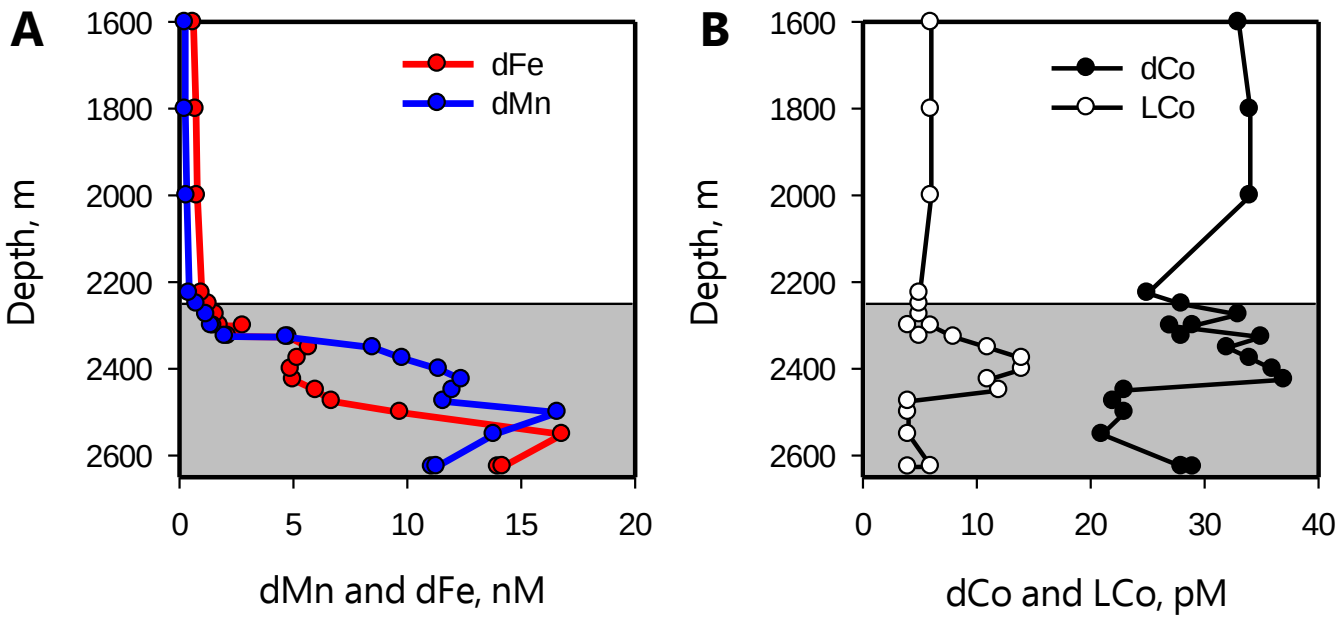
A
B
Depth, m
1600
1800
2000
2200
2400
2600
dFe
dMn
0
5
10
15
20
dMn and dFe, nM
dCo
LCo
10
20
30
40
dCo and LCo, pM

Figure 13

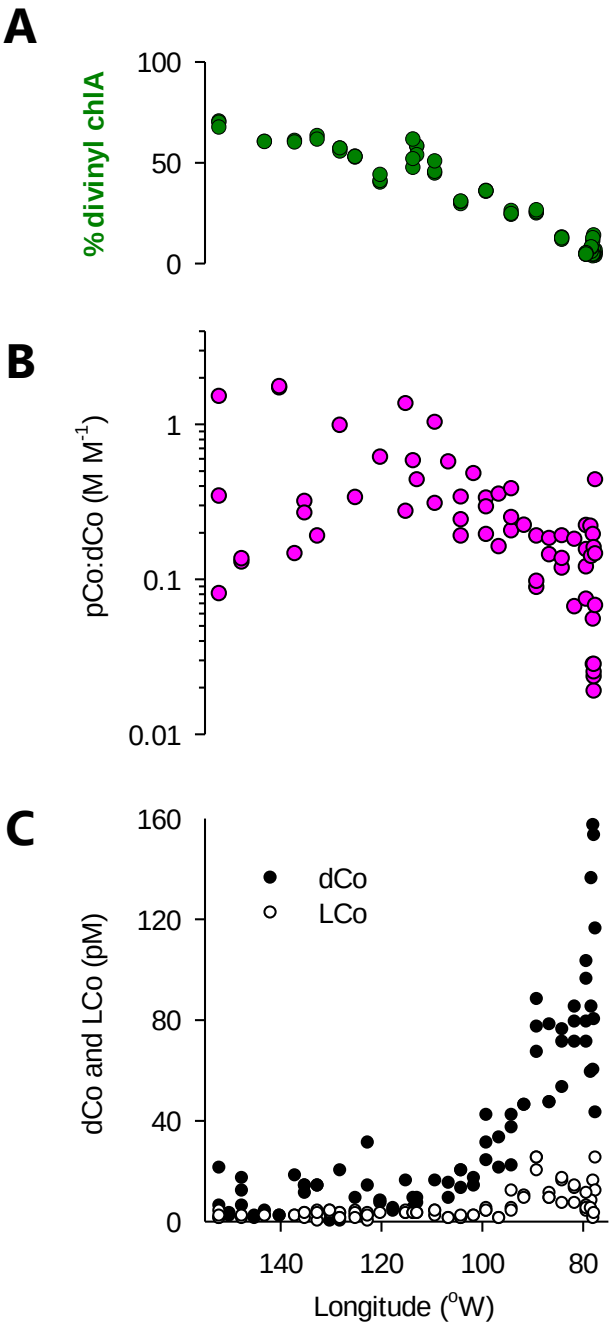
A
%divinyl chlA
100
50
0
B
pCo:dCo (M M-1)
1
0.1
0.01
C
dCo and LCo (pM)
160
120
80
40
0
dCo
LCo
140
120
100
80
Longitude (°W)

Figure 14

coastal source
uptake/export
remin. – scav.
phosphate
cobalt
uptake/export
gas exchange
remin. – scav.
coastal source
oxygen
cobalt
coastal source
upwelling
remin.
OMZ
uptake/export
remin.
gyre subduction
scavenging